DISSERTATION THESIS

Optimal input - output selection for the control of flexible structures

ausgeführt zur Erlangung des akademischen Grades eines
Doktors der technischen Wissenschaften
unter der Leitung von

Ao.Univ.Prof. Dipl.-Ing. Dr.techn. Martin Kozek

am Institut für Mechanik und Mechatronik
Abteilung für Regelungstechnik und Prozessautomatisierung

eingereicht an der Technischen Universität Wien
Fakultät für Maschinenbau

von

Dipl.-Ing. Mark Hemedi

Matr.-Nr. 0526336

Wien, im Oktober 2015

Abstract

In context of robust control design, this dissertation thesis deals with optimal input-output selection methods for flexible structures. New strategies are introduced. Assuming flexible structures with numerous input- and output candidates a meaningful choice is a basic prerequisite for an effective control design.

After an introduction into flexible structures topic, modelling and overview on the state of the art selection criteria the newly proposed input-output selection techniques are presented. Their properties and benefits are discussed. The methods are applied to a simple academic example to show their functionality. Evaluated results are verified by a standard criterion.

The applicability of proposed techniques to a high complex systems is shown by considering of two large "Blended Wing Body" aircraft models. The optimal input-output selection with respect to a control goal is carried out.

After conclusion an information on the ACFA 2020 Project is briefly given.

Kurzfassung

Die vorliegende Dissertationsarbeit befasst sich, im Kontext der robusten Regelung, mit Methoden zur optimalen Auswahl von Ein- und Ausgängen für flexible Strukturen und stellt neue Strategien vor. Im Fall zahlreicher Ein- und Ausgangskandidaten, ist eine effiziente Auswahl eine grundlegende Voraussetzung für ein effektives Regelkreis.

Nach der Einführung in das Thema von flexiblen Strukturen, Modellierung und Überblick über existierende Selektionsmethoden, werden die neu vorgeschlagenen Ein- und Ausgangssuchkriterien präsentiert. Ihre Eigenschaften sowie auch Vorteile werden diskutiert. Die Anwendbarkeit ist an einem akademischen Beispiel demonstriert. Berechnete Ergebnisse sind durch ein anerkanntes Standardkriterium verifiziert. Die Nützlichkeit der neu entwickelten Methoden für Systeme mit hoher Komplexität wird anschließend gezeigt. Die optimale Wahl der Ein- und Ausgänge für zwei "Blended Wing Body" Flugzeugmodelle, welche das Regelungsdesign mit gesetzten Regelzielen er-möglichen, werden berechnet.

Nach der Zusammenfassung im letzten Teil dieser Arbeit, werden grundlegende Informationen über das ACFA 2020 Projekt zusammengefasst.

Preface

This dissertation thesis was elaborated within the European Commission (EC)-funded research project ACFA 2020 (Active Control of a Flexible 2020 Aircraft). The project covered several engineering topics related to design of ultra modern blended wing civil aircraft concept. The outcome was a pre-design model for 450 passengers including a multi-objective control concept. I had the honour to participate in this challenging project and to contribute by my research on the optimal input-output selection problem, which is a key issue related to robust control design.

This dissertation thesis could be elaborated thanks to support from members of the Institute of Mechanics and Mechatronics, Division of Control and Process Automation at TU Wien where, in a pleasant and friendly atmosphere, great engineering challenges like the ACFA2020 project are being investigated. Many thanks go to Ao.Univ.Prof. Dipl.-Ing. Dr.techn. Martin Kozek and to Dipl.-Ing. Dr.techn. Alexander Schirrer for their guidance and valuable inputs. Special thanks go to my family for standing by me and supporting me not only during the doctoral studies but throughout my entire life.

Mark Hemedi

To my family

Contents

List of Figures

List of Tables

Chapter 1

Introduction

1.1 Work summary

In the context of flexible structure control, this thesis contributes with methods for optimal input/output (I/O) selection. Focusing on flexible structures with numerous I/O candidates, an optimal I/O selection is a basic prerequisite for a meaningful control design thus it deserves a serious attention before main control design starts. The goal is to find an appropriate locations on the flexible structure which will allow the controller to measure and manipulate it's dynamics most effectively, namely, to damp oscillations excited by process disturbances across all predefined frequency range.

The main contribution of this thesis are newly developed I/O selection criteria. Their attributes are discussed. Proposed I/O selection techniques are applied to a simple flexible structures as well as to high complex industrial systems. The results are validated by another reference criteria. It is shown that the proposed techniques compute consistent results. Their properties and advantages are outlined.

An advanced I/O selection method proposed by this thesis is based on designing of an energetically equivalent LQG sub-loops. These sub-loops use single inputs and outputs, eventually sets of them. A prescribed controller norm referring to it's available energy resources is met iteratively during control design. Finally, a performance index is assigned to the investigated I/Os . Similarly, the performance indexes for the remaining I/O combinations are evaluated and finally, preferred I/Os for the main control design are highlighted.

The system weighting matrices can be implemented right at the beginning of the I/O selection process. Hence, the initial knowledge of the system and process

disturbances can be easily incorporated. This criterion computes a reliable and meaningful results. It has been published on 17^{th} Mediterranean Conference on control & Automation ([20]). Moreover, it is confronted with another reference I/O selection method given in [4]. Their properties and contrasts are discussed (see also [19]).

Another proposed open-loop I/O selection technique deals with parameter varying systems. Assuming that the fine discretized plant represents the system dynamics in it's all relevant operating points, this method selects I/O candidates which allow to design a robustly performing control loop. It is based on elimination principle. It consists of three main subsequent steps, whereas each step contains specific properties related to phase difference and peak magnitude. Those I/O pairs which do not satisfy requirements stated therein are eliminated for further consideration. A few presumed best performing candidates are then highlighted. This criterion is well applicable to systems with high complexity and with a high number of candidates. It was introduced on 10^{th} International Conference on Motion and Vibration Control in Tokyo ([21]), moreover, presented technique has been submitted to the Journal of System Design and Dynamics (JSDD) and published by Japan Society of Mechanical Engineers (JSME, see [22]).

Usability of proposed I/O selection methods for a large and high complex systems is demonstrated by a case study of blended wing body aircraft type. This thesis emphasises the relevancy of the optimal I/O selection step in overall control design, brings new methods and points at their advantages.

1.2 Introduction to the I/O selection topic

The task of control design is often perceived as starting out with a given multi-input multi-output (MIMO) plant model. This reduces the view on carrying out the control architecture. As stated in standard textbooks [40] and [47], the control design is a complex process where each step is essential. Even initial conditions like precision of modelling, uncertainty definition or system order reduction accuracy, play a relevant role for the control engineer and will be reflected in performance of the implemented control law.

As outlined in [41], [20] as well as in [21], a vital task in the context of system control design is the optimal input-output (I/O) selection. Considering a MIMO plant layout (see Fig.1.1), the goal is to select a subset of inputs and outputs, which indicate specific desired attributes based on system open loop properties and physical insight information.

In general, a subset of plant inputs is sought which transfers sufficient amount of energy into the plant to manipulate it and to keep it in desired conditions. Attractive plant outputs are those which allow accurate observation of information about the plant dynamics. If a parameter varying system is investigated, selected I/Os have to allow to control the plant over all relevant parameter range. A general control goal is to keep the influence of disturbance w on controlled variable z in predefined operating points in acceptable limits (see Fig. 1.1).

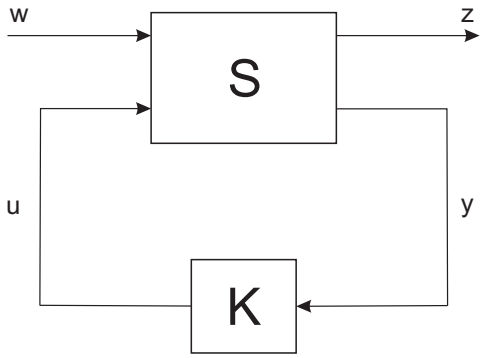

Figure 1.1: General control loop layout; S is the MIMO plant; K is the controller; w is the process disturbance; z is the controlled variable; u are the controlled plant inputs; y are the measured plant outputs

In the following text, the flexible structure is assumed to be the plant to be controlled. Process disturbances may cause undesired effects which need to be com-

pensated by a control loop. One of the most relevant properties of flexible structures is their resonance. It is basically a strong amplification of motion at a specific excitation frequency. This frequency is called natural or eigenfrequency. There are several frequencies that structures resonance at. The structure movement at these frequencies forms a specific shape. Each eigenfrequency is explicitly associated with the corresponding structure shape which remains, in the linear case, the same pattern of deformation. This shape of oscillating structure at it's natural frequency is called a mode shape or a structural mode. The structural modes are typically considered. If their damping is sufficiently low and they are sufficiently spaced in frequency ([10]) they can be excited separately. This is one of the most important flexible structure characteristics from an engineering point of view.

In some disciplines, the resonances are desired (e.g. acoustics). In the context of this work, the resonances pose an undesired behaviour and need to be damped. In many technical applications the structure vibrations and resonances excited by disturbances can lead to structural stress, material fatigue, noise emissions, inconstant force transmission, shortening of lifetime, defects, plant checks may be needed more frequently, etc. Mentioned effects show that considering natural frequencies deserves a serious attention.

Modern engineering tries to fix these problems not only by increasing of passive damping, or by shifting system eigenfrequencies out of the operation points, but in recent years active damping concepts became highly popular in many disciplines due to their specific performance potential.

Active vibration control techniques expand quickly and find their application in various engineering fields (skyscrapers, convertible car chassis, latest aeronautical technologies, etc.).

Progressive innovations in structure control as well as new, highly sophisticated approaches and tools are being developed in order to offer new engineering solutions to the market.

1.3 Work structure

This dissertation thesis is structured as follows: the I/O selection problem is introduced in Sec.1.2. The flexible structures and their basic properties are briefly discussed in Sec.2.1. Preparation of mathematical system models is shown in Sec.2.2.

An overview on existing state-of-the-art I/O selection methods is given in Sec.2.3. A reference energy-based I/O selection approach according to [10] can be found in Sec.3.1. New I/O selection technique based on energetically equivalent closed subloops is presented in Sec.3.2. In Sec.3.3, two LQG-based criteria are compared and discussed. Another proposed I/O selection criterion for systems with varying parameter is discussed in and Sec.3.4. Developed criteria are applied to an elementary academic example and their practicability is validated in Sec.4. Sec.5 deals with a case study of an industrial application. After a short overview on flight vehicle evolution in Sec.5.1, the Blended Wing Body aircraft type is outlined. Benefits and expectations are briefly summarized. The "NACRE" model is presented in Sec.5.2 and related optimal I/O selection results are given in Sec.5.3. The "ACFA" model is discussed in 5.4. I/O selection results related to this model are given in Sec.5.5. Sec.6 summarizes the main findings and content of this work. In the Apendix, an overview on the ACFA2020 project is briefly given.

Chapter 2

Flexible structures, modelling and standard I/O selection techniques

In this chapter an overview on flexible structures' and it's main characteristics is discussed. A mathematical modelling in nodal as well as in modal coordinates is outlined. An overview on state of the art I/O selection techniques is given as well.

2.1 Definition of a flexible structure system

In the context of this work, the term flexible structure is used for a linear system, which is

- finite-dimensional,
- controllable and observable,
- has poles exclusively as distinct, weakly-damped, complex-conjugate pairs,
- does not show clustered poles.

Their basic properties are assumed as:

- Motion of flexible structures can be described by the representation of decoupled modes.
- Each structural mode can be excited separately without exciting the remaining ones.
- Displacement signals of each point of the structure are sinusoidal with fixed frequencies.

- The shape of the structural deformation at a natural frequency is called "mode shape".
- In the Laplace domain (s plane), the system poles are conjugate (see Fig. 2.1).
- Small real parts refer to low structural damping (see Fig. 2.2).
- Resonance peaks are present in the transfer function (see Fig. 2.3)
- The impulse response consists of harmonic components related to complex poles

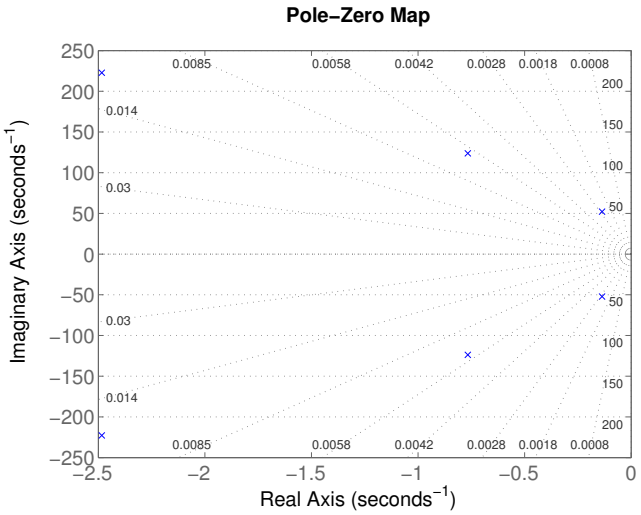

Figure 2.1: Pole-zero map of a system with 6 states (3 modeled eigenfrequencies)

Each pair of system conjugate poles refers to one eigenfrequency. In general, according to the following diagram (see Fig.2.2 and [30] for more detail), a stable system with conjugate poles resonates at frequency ω_d which is the damped natural frequency. The undamped natural frequency ω_n is equal to the length of the vector P. Cosine of the angle between vector P and negative real axis is equal to damping ratio ζ.

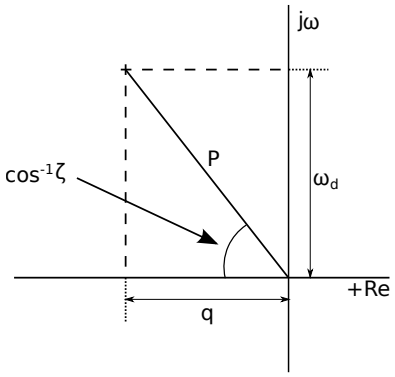

Figure 2.2: Pole, its damped and undamped natural frequencies and damping ratio ζ

These vector components have following relations:

$$\omega_d{}^2 = \omega_n{}^2 - \omega_n{}^2\zeta^2 \tag{2.1}$$

$$\omega_d = \omega_n\sqrt{1-\zeta^2} \tag{2.2}$$

The Bode diagram shows the system response in the frequency domain. Each peak represents a system resonance (the first three eigenfrequencies of a structures's transfer function are shown in Fig.2.3).

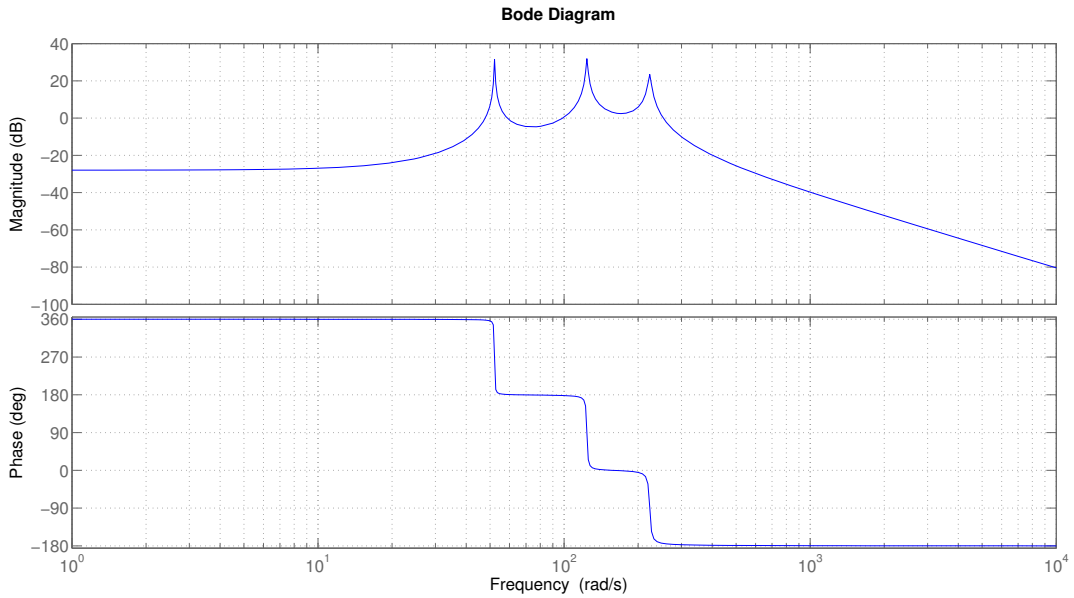

Figure 2.3: Resonance peaks

In the following text a standard mathematical modelling approach for flexible structure dynamics is outlined. Nodal coordinates, modal coordinates as well as their state space formulation are given.

2.2 Structure modelling

It is assumed that all structural dynamics discussed here are stable and linear with proportional damping. The dynamics of flexible structures are often described by n linear (or linearized) equations of motion. The commonly used mathematical model can be represented by a set of n 2^{nd} order linear ordinary differential equations (ODEs). A crucial decision for further investigation and model handling is the choice of their coordinates. The coordinates in which the system is being described is chosen arbitrarily. Two coordinate systems are commonly used:

- nodal coordinates
- modal coordinates

When using nodal coordinates, displacements and velocities of defined structural points, (nodes) are directly represented as the degrees of freedom.
Modal coordinates, on the other hand, consider displacements and velocities of structural modes (eigenshapes - patterns of deformation at certain eigenfrequencies).
Note that the transfer functions of the system for particular inputs and outputs must remain invariant with respect to the choice of coordinates.

A good starting point for modelling of flexible structure is a linearized model described by its mass, stiffness and damping matrices and in addition, by actuation and measurement locations (I/Os). Typically, so-called nodal models can be retrieved in nodal coordinates (displacements and velocities) by FE modelling. The linear equations of motion are commonly written in the following 2^{nd} order form:

$$\begin{aligned} \boldsymbol{M}\ddot{\boldsymbol{q}}_{\mathrm{n}}(t) + \boldsymbol{D}\dot{\boldsymbol{q}}_{\mathrm{n}}(t) + \boldsymbol{K}\boldsymbol{q}_{\mathrm{n}}(t) &= \boldsymbol{B}\boldsymbol{u}(t) \\ \boldsymbol{y} &= \boldsymbol{C}_{oq}\boldsymbol{q}_{\mathrm{n}}(t) + \boldsymbol{C}_{ov}\dot{\boldsymbol{q}}_{\mathrm{n}}(t), \end{aligned} \tag{2.3}$$

where $\boldsymbol{M} > 0$, $\boldsymbol{D} \geq 0$, and $\boldsymbol{K} \geq 0$ are $(n \times n)$ mass-, damping-, and stiffness matrices discretized and modelled by n nodal degrees of freedom, $\boldsymbol{q}_{\mathrm{n}}(t)$, $\dot{\boldsymbol{q}}_{\mathrm{n}}(t)$, and $\ddot{\boldsymbol{q}}_{\mathrm{n}}(t)$ are the $(n \times 1)$ nodal displacement vector and its time derivatives ($\boldsymbol{M} > 0$ denotes strict positive-definiteness). The $(n \times s)$ $\boldsymbol{B}$ matrix defines the effect of generalized input forces on the nodal degrees of freedom (generalized displacements). The $(s \times 1)$ input vector $\boldsymbol{u}(t)$ represents the input channels. The $(r \times n)$ output displacement matrix $\boldsymbol{C}_{oq}$ and output velocity matrix $\boldsymbol{C}_{ov}$ define the $(r \times 1)$ output vector $\boldsymbol{y}$. In the following, the notion of explicit time dependence is omitted. This system of coupled

2^{nd} order ODEs can be rewritten into a system of $1st$ order ODEs in state space form by defining the state space vector as a linear combination of the structural displacements $\boldsymbol{q}_{\mathrm{n}}$ and velocities $\dot{\boldsymbol{q}}_{\mathrm{n}}$:

$$\boldsymbol{x}_n = \begin{bmatrix} \boldsymbol{q}_{\mathrm{n}} \\ \dot{\boldsymbol{q}}_{\mathrm{n}} \end{bmatrix} \tag{2.4}$$

Then the state equation reads:

$$\dot{\boldsymbol{x}}_{\mathrm{n}} = \begin{bmatrix} \boldsymbol{0}_{[n\times n]} & \boldsymbol{I}_{[n\times n]} \\ -\boldsymbol{M}^{-1}\boldsymbol{C} & -\boldsymbol{M}^{-1}\boldsymbol{K} \end{bmatrix} \boldsymbol{x}_{\mathrm{n}} + \begin{bmatrix} \boldsymbol{0}_{[n\times r]} \\ \boldsymbol{M}^{-1}\boldsymbol{B} \end{bmatrix} \boldsymbol{u} \tag{2.5}$$

with $\boldsymbol{0}$ and $\boldsymbol{I}$ as zero and unity matrices, respectively, with the indicated dimensions. The system output can be written as:

$$\boldsymbol{y} = \begin{bmatrix} \boldsymbol{C}_{oq} & \boldsymbol{C}_{ov} \end{bmatrix} \boldsymbol{x}_{\mathrm{n}} \tag{2.6}$$

Thus, the general state space form is obtained:

$$\begin{aligned} \dot{\boldsymbol{x}}_{\mathrm{n}} &= \boldsymbol{A}_{\mathrm{n}}\boldsymbol{x}_{\mathrm{n}} + \boldsymbol{B}_{\mathrm{n}}\boldsymbol{u} \\ \boldsymbol{y} &= \boldsymbol{C}_{\mathrm{n}}\boldsymbol{x}_{\mathrm{n}} \end{aligned} \tag{2.7}$$

Modal models of structures are described by modal coordinates and exhibit favourable properties. They can be derived from nodal models by using the $(n \times n)$ matrix of eigenfunctions (mode shapes) $\boldsymbol{\Phi}$ of the undamped generalized eigenvalue/eigenvector problem $\boldsymbol{K}\boldsymbol{\phi}_i = \omega_i^2 \boldsymbol{M}\boldsymbol{\phi}_i$ for state transformation and subsequent reordering and scaling [10]. The 2^{nd} order model (Eqn.2.3) becomes:

$$\begin{aligned} \boldsymbol{M}_{\mathrm{m}}\ddot{\boldsymbol{q}}_{\mathrm{m}} + \boldsymbol{D}_{\mathrm{m}}\dot{\boldsymbol{q}}_{\mathrm{m}} + \boldsymbol{K}_{\mathrm{m}}\boldsymbol{q}_{\mathrm{m}} &= \boldsymbol{\Phi}^T\boldsymbol{B}_o\boldsymbol{u} \\ \boldsymbol{y} = \boldsymbol{C}_{oq}\boldsymbol{\Phi}\boldsymbol{q}_{\mathrm{m}} + \boldsymbol{C}_{ov}\boldsymbol{\Phi}\dot{\boldsymbol{q}}_{\mathrm{m}} \end{aligned} \tag{2.8}$$

with the diagonal modal mass-, damping-, and stiffness-matrices $\boldsymbol{M}_{\mathrm{m}} = \boldsymbol{\Phi}^T\boldsymbol{M}\boldsymbol{\Phi}$, $\boldsymbol{D}_{\mathrm{m}} = \boldsymbol{\Phi}^T\boldsymbol{D}\boldsymbol{\Phi}$ (diagonal in the commonly assumed case of Rayleigh-damping), and $\boldsymbol{K}_{\mathrm{m}} = \boldsymbol{\Phi}^T\boldsymbol{K}\boldsymbol{\Phi}$, respectively.

By state reordering and further transformations (refer to [10] for details), one arrives at the modal state-space model. The state vector for each mode i is chosen

as $\boldsymbol{x}_{\mathrm{m}i} = \begin{bmatrix} \omega_i q_{\mathrm{m}i} \\ \dot{q}_{\mathrm{m}i} \end{bmatrix}$, whereas ω_i is the i^{th} natural frequency. The system is decoupled mode-wise, thus the system matrix $\boldsymbol{A}_{\mathrm{m}}$ is (2×2) block-diagonal with blocks $\boldsymbol{A}_{\mathrm{m}i}$ for each mode i:

$$\begin{aligned} \boldsymbol{A}_{\mathrm{m}i} &= \begin{bmatrix} 0 & \omega_i \\ -\omega_i & -2\zeta_i\omega_i \end{bmatrix} \qquad \boldsymbol{B}_{\mathrm{m}i} = \begin{bmatrix} \boldsymbol{0} \\ \boldsymbol{b}_{\mathrm{m}i} \end{bmatrix} \\ \boldsymbol{C}_{\mathrm{m}i} &= \begin{bmatrix} \frac{\boldsymbol{c}_{\mathrm{mq}i}}{\omega_i} & \boldsymbol{0} \end{bmatrix} \end{aligned} \tag{2.9}$$

where ζ_i stands for modal damping of i^{th} mode.

$$\begin{aligned} \boldsymbol{A}_{\mathrm{m}} &= \mathrm{diag}\left(\boldsymbol{A}_{\mathrm{m}i}\right) \qquad \boldsymbol{B}_{\mathrm{m}} = \begin{bmatrix} \boldsymbol{B}_{\mathrm{m}1} \\ \boldsymbol{B}_{\mathrm{m}2} \\ \vdots \\ \boldsymbol{B}_{\mathrm{m}n} \end{bmatrix} \\ \boldsymbol{C}_{\mathrm{m}} &= \begin{bmatrix} \boldsymbol{C}_{\mathrm{m}1} & \boldsymbol{C}_{\mathrm{m}2} & \dots & \boldsymbol{C}_{\mathrm{m}n} \end{bmatrix}. \end{aligned} \tag{2.10}$$

The general modal state space model reads:

$$\begin{aligned} \dot{\boldsymbol{x}}_{\mathrm{m}} &= \boldsymbol{A}_{\mathrm{m}}\boldsymbol{x}_{\mathrm{m}} + \boldsymbol{B}_{\mathrm{m}}\boldsymbol{u} \\ \boldsymbol{y} &= \boldsymbol{C}_{\mathrm{m}}\boldsymbol{x}_{\mathrm{m}} \end{aligned} \tag{2.11}$$

One of the main reasons to use the modal state space representation is that in case of high order nodal models (as obtained via FE modelling), the order can easily be reduced in the modal representation by truncating higher modes without significantly changing system behaviour. Also, the obtained set of modes is orthogonal (in the weakly damped case), which allows to break down the complexity of operations and system treatment considerably.

Consider a non-linear system, described in a general state space formulation:

$$\begin{aligned} \dot{\boldsymbol{x}} &= \boldsymbol{f}\left(\boldsymbol{x}, \boldsymbol{u}, \boldsymbol{\Theta}\right) \\ \boldsymbol{y} &= \boldsymbol{g}\left(\boldsymbol{x}, \boldsymbol{u}, \boldsymbol{\Theta}\right), \end{aligned} \tag{2.12}$$

where it is assumed that all major non-linearities can be mapped into the parameter vector $\boldsymbol{\Theta}$. By computing the system's Jacobians with respect to states, inputs, and outputs,

$$\begin{aligned} \boldsymbol{A}(\boldsymbol{\Theta}) &= \left.\frac{\partial \boldsymbol{f}}{\partial \boldsymbol{x}}\right|_{(\boldsymbol{x}_0,\boldsymbol{u}_0,\boldsymbol{\Theta})} & \boldsymbol{B}(\boldsymbol{\Theta}) &= \left.\frac{\partial \boldsymbol{f}}{\partial \boldsymbol{u}}\right|_{(\boldsymbol{x}_0,\boldsymbol{u}_0,\boldsymbol{\Theta})} \\ \boldsymbol{C}(\boldsymbol{\Theta}) &= \left.\frac{\partial \boldsymbol{g}}{\partial \boldsymbol{y}}\right|_{(\boldsymbol{x}_0,\boldsymbol{u}_0,\boldsymbol{\Theta})} & \boldsymbol{D}(\boldsymbol{\Theta}) &= \left.\frac{\partial \boldsymbol{g}}{\partial \boldsymbol{u}}\right|_{(\boldsymbol{x}_0,\boldsymbol{u}_0,\boldsymbol{\Theta})}, \end{aligned} \tag{2.13}$$

the nominal linearized systems at the operating points $(\boldsymbol{x}_0, \boldsymbol{u}_0, \boldsymbol{\Theta} = \boldsymbol{\Theta}_0)$ can be defined. Here, it is assumed that no feedthrough term exists ($\boldsymbol{D} = \boldsymbol{0}$), which is fulfilled for structure models if the outputs are linear combinations of the states only (i.e. displacements or velocities) and if truncation methods were used for state reductions (see [40] for a discussion on reduction techniques). Acceleration sensors (leading to non-zero $\boldsymbol{D}$) can be incorporated by according transformations under the condition that the original system exhibits zero feedthrough (see [10]).

Further model handling (e.g. preparation for control design stage) might require some specific input, output, or mode prioritisation. This can be related to available a priori knowledge, such as operation frequency range, constructional layout, etc.
A general, yet simple solution to incorporating design constraints and conditions into system analysis using different methods is to apply a physically motivated I/O weighting to the system model. For modal system representations, also per-mode weights can be incorporated easily if the weights fulfil mild regularity conditions (see [10]).

Let $(\boldsymbol{A}_\mathrm{m}, \boldsymbol{B}_\mathrm{m}, \boldsymbol{C}_\mathrm{m})$ be a modal MIMO state-space system description of an unweighted system (Eqn.2.11), $\boldsymbol{G}(j\omega)$ a scalar transfer function describing a frequency weighting. Then, under the regularity conditions stated in [10], a frequency-weighted input matrix $\boldsymbol{B}_\mathrm{m,w}$ can be constructed mode-wise (for mode i, where *i=1,2,3,...*) using the weighting function value at each mode's frequency:

$$\boldsymbol{B}_{\mathrm{m}i,\mathrm{w}} = \begin{bmatrix} \boldsymbol{0} \\ \boldsymbol{b}_{\mathrm{m}i} G(j\omega_i) \end{bmatrix} \tag{2.14}$$

Likewise, frequency weighting of outputs and per-input or per-output weightings can be realized and combined into the scaled system $(\boldsymbol{A}_\mathrm{m,w}, \boldsymbol{B}_\mathrm{m,w}, \boldsymbol{C}_\mathrm{m,w})$ with unchanged modal properties; the mode gains are adapted to implement the physi-

cal system weighting. This allows to skip any further weighting in the subsequent methods, enabling comparative analysis of the same underlying model.

For further system treatment it can be crucial to correctly formulate and incorporate relevant design constraints or conditions. These can be, for example, the expected excitation spectra for vibration control design, performance quantity weighting (e.g. weighted accelerations are used to estimate passenger ride comfort), or an actuator efficiency quantity.

2.3 Overview on state-of-the-art I/O selection methods

The field of I/O selection is large, and many strategies exist in literature. The survey article [42] gives a broad, structured overview on state-of-the art I/O selection approaches and criteria.

One class of approaches is of qualitative nature. A criterion of accessibility given in [13], in which causal paths between manipulated or controlled and measured variables have to exist.

Another approach given in [7] supports non-linear models and uses the relative degree r_{ij} of a controlled variable y_i with respect to a manipulated variable u_j as a measure of the dynamic interaction. In this way, the direct effect of manipulated variables on controlled variables is assessed.

Amongst the quantitative approaches, a family of I/O selection criteria is based on state controllability and observability, given for example in [47] or [24].

Grammian-based methods seek to optimally condition the observability/controllability grammian eigenvalues. Examples are in [12] or [15] (which is well applicable to flexible structures since it provides a balance between the importance of lower and higher order modes).

The balanced form of a stable, controllable, and observable plant and its Hankel singular values (HSV) are used as criterion in [11] and [37], and extended by performance weights in [33]. References [31] and [10] assess the state controllability and observability in a weighted sense. The approach presented in [43] exploit their individual advantages. The I/O selection procedure proposed in [20] is based on a normalized comparison of LQG closed loops, which are designed for each I/O candidate separately.

A comparison of two LQ-based I/O selection criteria is given in [19]. An optimal

selection method for systems with varying parameter is given in [21] as well as in [22]. This procedure is based on reduction of I/O candidates which does not satisfy criteria predefined in elimination steps.

A different method, called right half-plane zeros positioning strategy, is described in [8], [47], and others.

Another group of concepts assess the efficiency of manipulation and estimation. Their key idea is to minimize input-set (output-set) dependent cost functions J_u (J_y) in terms of minimal input energy (maximum system information), see [2] and [38].

An extension to non-linear systems is given in [5]. In order to minimize the state estimation error, a Kalman filter is used in [28], minimizing J_y.

Optimal I/O selection methods based on the Fisher information matrix are given in [17], [18] and [16].

Chapter 3

Optimal I/O selection methods

In this chapter, I/O selection criteria are discussed in detail. The Method A, a standard criterion according to [10] is explained in Sec.3.1. In Sec.3.2 a newly proposed criterion, the Method B based on comparison of closed loops, is presented (see [20]). For each I/O candidate, an energetically equivalent LQG closed loop design is carried out and a performance index is evaluated. This performance index refers to the candidate's suitability. Best performing candidates for a simple flexible beam structure in hinged-hinged configuration evaluated by this method are shown in Sec.4.2.
Sec.3.3 compares, qualitatively and quantitatively, the Method B (Sec.3.2) with the Method C - another LQ based I/O selection approach using LMI methods which is given in [4]. Attributes of both methods are discussed. Both selection techniques are applied to the same academic example and the selection results are carried out. They are shown in Sec.4.3.
Next newly suggested I/O selection technique, the Method D is introduced in Sec.3.4. It deals with parameter depending systems. It seeks optimal I/O candidates which allow to design a robustly performing controller and thus compensate process disturbances across the entire relevant parameter range. This criterion consists of three eliminations substeps. In each substep those I/Os are eliminated which do not fulfil given requirements. A performance index is assigned to the remaining I/Os. This selection method is applied to a simple flexible beam in hinged-hinged and hinged-clamped configurations and optimal positions are found. Results are given in Sec.4.4.

3.1 Method A - Energy-based I/O selection criterion

In this section, the selection strategy stated in [10] is discussed. Consider a flexible dynamical system with $j = 1..A$ input positions and a fixed set of outputs S, see Fig. 3.1. The bold blue arrow represents the single actuation (j) while all yellow labelled outputs (set S) are considered.

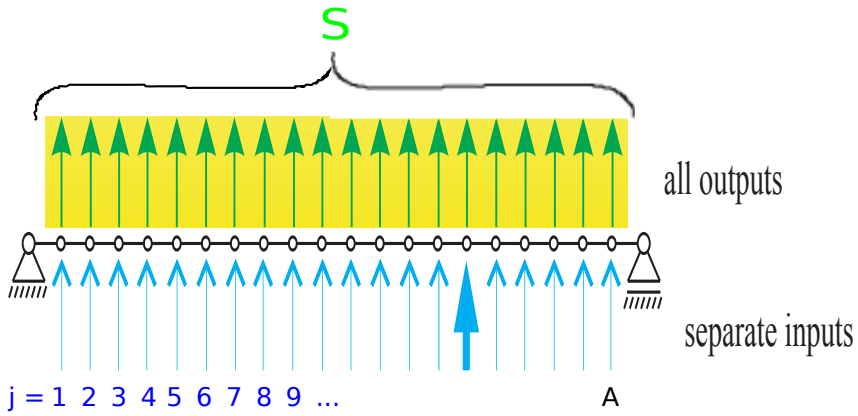

Figure 3.1: Schematic diagram of flexible beam

In case of well-separated weakly damped eigenmodes (represented in modal coordinates), each mode i is independent with respect to the other modes. Consequently, also the single mode norms are independent. This allows to consider each mode separately.

The single-actuator modal norm $\|\boldsymbol{G}_{ij}\|_2$ of mode i of the system actuated by a single actuator j and the candidate set of sensors S, as well as the global modal norm of the fully actuated system $\|\boldsymbol{G}_i\|_2$ can be derived from the modal system matrices as:

$$\|\boldsymbol{G}_{ij}\|_2 = \frac{\|\boldsymbol{B}_{\mathrm{m}ij}\|_2 \|\boldsymbol{C}_{\mathrm{m}i}\|_2}{2\sqrt{\zeta_i \omega_i}} \tag{3.1}$$

$$\|\boldsymbol{G}_i\|_2 = \sqrt{\sum_{j \in A} \|\boldsymbol{G}_{ij}\|_2^2}, \tag{3.2}$$

where $\boldsymbol{B}_{\mathrm{m}ij}$ is the (2×1) block of the j-th input (actuator) of the input matrix $\boldsymbol{B}_{\mathrm{m}i}$ for mode i and $\boldsymbol{C}_{\mathrm{m}i}$ contains the fixed sensor set S for mode i. Likewise, the single-sensor modal norm $\|\boldsymbol{G}_{ik}\|_2$ of mode i of the fully actuated system, sensed by a single sensor k can be formulated in a similar manner.

The $\mathcal{H}_2$ norm of a strictly proper, stable linear SISO system with transfer function $G(s)$ is defined as:

$$\|\boldsymbol{G}\|_2 = \left(\frac{1}{2\pi}\int_{-\infty}^{\infty} |G(j\omega)|^2 d\omega\right)^{\frac{1}{2}} \tag{3.3}$$

For a MIMO system with transfer function matrix $\boldsymbol{G}(s) = [g_{kl}(s)]$, the definition of the $\mathcal{H}_2$ norm can be written as follows:

$$\|\boldsymbol{G}\|_2 = \left(\sum_{kl} \|g_{kl}\|_2^2\right)^{\frac{1}{2}} \tag{3.4}$$

$$= \left(\frac{1}{2\pi}\int_{-\infty}^{\infty} \sum_{kl} |g_{kl}(j\omega)|^2 d\omega\right)^{\frac{1}{2}} \tag{3.5}$$

$$= \left(\frac{1}{2\pi}\int_{-\infty}^{\infty} \sum_{kl} g_{kl}(-j\omega) g_{kl}(j\omega) d\omega\right)^{\frac{1}{2}} \tag{3.6}$$

$$= \left(\frac{1}{2\pi}\int_{-\infty}^{\infty} tr[\boldsymbol{G}(-j\omega)^T \boldsymbol{G}(j\omega)] d\omega\right)^{\frac{1}{2}} \tag{3.7}$$

Note that in this context the $\mathcal{H}_2$ norm is interpreted as average input (actuator case) / output (sensor case) mechanical energy transferred into / from the structure. Let denote by $\boldsymbol{G}_A$ the transfer function of the system actuated through all candidate inputs in A and $\boldsymbol{G}_S$ the transfer function of the system with all candidate outputs in S. By formulating the relative contribution of each actuator or sensor to the global mode norm, actuator selection indices σ_{ij} and sensor selection indices σ_{ik} are defined to evaluate the respective actuator/sensor importance for mode i:

$$\sigma_{\text{act},ij} = w_{ij}\frac{\|G_{ij}\|_2}{\|\boldsymbol{G}_A\|_2} \qquad \sigma_{\text{sens},ik} = w_{ik}\frac{\|G_{ik}\|_2}{\|\boldsymbol{G}_S\|_2}, \tag{3.8}$$

where $\boldsymbol{w}_{ij}$ and $\boldsymbol{w}_{ik}$ are additional design weights that can be assigned to the j-th actuator, respectively to the k-th sensor and mode i. All selection indices can be collected into a selection matrix:

$$\boldsymbol{\Sigma}_{\text{act}} = [(\sigma_{ij})] \qquad \boldsymbol{\Sigma}_{\text{sens}} = [(\sigma_{ik})] \tag{3.9}$$

These matrices describe the performance of each actuator j / sensor k (columns) separately with respect to each mode i (rows).

To obtain the aggregate selection index based on the $\mathcal{H}_2$ norm (see [10]), for each actuator/sensor column the root-mean-square sum over all modes (rows of $\mathbf{\Sigma}$) is computed. The resulting (row) vector shows the performance for each candidate actuator or sensor (e.g. $\mathrm{PI}_{\mathrm{Gaw},j} = \sqrt{\sum_{i=1}^{n} \sigma_{ij}^2}$ for actuator j). Due to the fact that the $\mathcal{H}_2$ norm of single modes (if considering displacement outputs) is typically decreasing with increasing mode number, the criterion is usually dominated by a few low order modes if no further mode weighting is introduced.

This, in effect, masks out virtually any effect of higher modes in the criterion. If the designer tries not only to maximize energy transfer efficiency, but also seeks positions that guarantee a minimum controllability of all higher modes, the criterion has to be extended accordingly (this is done in [44]).

Note that choosing the design weights w_{ij} or w_{ik} to incorporate physical constraints or conditions is not straightforward. One method with clear physical interpretation is to shift the weighting task into the system formulation itself, where input and output frequency weights can be applied directly per mode as outlined in Sec.2.2 (see also [10]).

3.2 Method B - LQG approach for I/O selection

A new concept for solving the actuator/sensor selection problem is discussed. Simplicity and high effectiveness render the following technique a powerful computational tool. The following method was published on the 17^{th} IEEE Mediterranean Conference on Control & Automation in Thessaloniki, Greece (see [20])

Although the system description (see Sec. 2.2) is decoupled per mode, the closed-loop design in the method below follows a general/comprehensive approach.

The main idea is to design comparable closed loop systems for each candidate actuator or sensor (see Fig. 3.2).

The closed-loops' performance is evaluated and then used as selection index. It is important to find a suitable property to establish comparable closed loops. This property, for example a fixed system norm quantity, is obtained by an iterative control design. Thus, the different closed-loop systems can be mutually compared in a normalized, "fair" way.

In the following, the method is realized for optimal actuator selection in a flexible structure system. As control design method, a modally weighted LQG design was

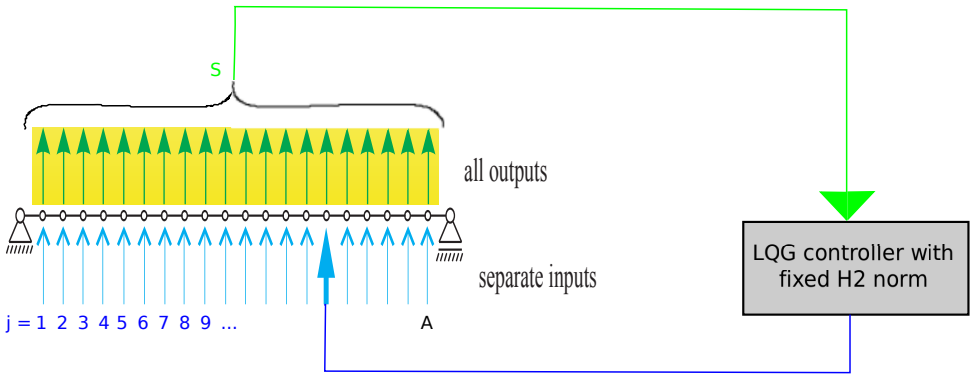

Figure 3.2: LQG control loop layout

applied.

Consider a system equipped with actuators and sensors where each investigated actuator and fixed set of sensors constitute one variant. In the LQ regulator (LQR) design, a quadratic cost function is being minimized:

$$J(\boldsymbol{x},\boldsymbol{u}) = \mathrm{E}\left\{\lim_{T\to\infty}\frac{1}{T}\int_0^T \left(\boldsymbol{x}^T\boldsymbol{Q}\boldsymbol{x} + \boldsymbol{u}^T\boldsymbol{R}\boldsymbol{u}\right)\mathrm{d}t\right\} \tag{3.10}$$

where $\boldsymbol{x}$ denotes system states and $\boldsymbol{u}$ is reserved for system inputs. In the standard LQR control design, $\boldsymbol{Q}$ and $\boldsymbol{R}$ are appropriately chosen constant weighting matrices which fulfil that $\boldsymbol{Q} = \boldsymbol{Q}^T$ and $\boldsymbol{R} = \boldsymbol{R}^T > \boldsymbol{0}$. The solution of the LQR problem consists of determining linear quadratic regulator $\boldsymbol{K_r}$, which is a constant matrix.

In general, consideration of an LGQ (Linear-quadratic Gaussian) design means to compute an appropriate state estimator and optimal feedback state regulator. An essential step in the LQG control design is the state estimator synthesis. The optimal state estimate is performed by Kalman filtering which is independent from weighting matrices $\boldsymbol{Q}$ and $\boldsymbol{R}$. It is assumed that the plant dynamics is linear (or linearized) and that the noise signals $\boldsymbol{w}$ and $\boldsymbol{v}$ are uncorrelated zero-mean Gaussian stochastic processes with known constant covariance matrices $\boldsymbol{W} = \mathrm{E}\left\{\boldsymbol{w}\boldsymbol{w}^T\right\}$ and $\boldsymbol{V} = \mathrm{E}\left\{\boldsymbol{v}\boldsymbol{v}^T\right\}$ where $\mathrm{E}\{\}$ denotes the expected value operator. The control design task is to find a control law

$$\boldsymbol{u} = -\boldsymbol{K}\hat{\boldsymbol{x}} \tag{3.11}$$

that minimizes the closed-loop objective in Eqn.3.10.

The optimal state estimates $\hat{\boldsymbol{x}}$ are obtained by a Kalman state estimator which has

the structure of ordinary state-observer:

$$\dot{\hat{\boldsymbol{x}}} = \boldsymbol{A}\hat{\boldsymbol{x}} + \boldsymbol{B}\boldsymbol{u} + \boldsymbol{L}(\boldsymbol{y} - \boldsymbol{C}\hat{\boldsymbol{x}}) \tag{3.12}$$

and whose gain (which minimizes $E\{[\boldsymbol{x} - \hat{\boldsymbol{x}}]^T[\boldsymbol{x} - \hat{\boldsymbol{x}}]\}$) is

$$\boldsymbol{L} = \boldsymbol{Y}\boldsymbol{C}^T\boldsymbol{V}^{-1} \tag{3.13}$$

with the solution $\boldsymbol{Y} = \boldsymbol{Y}^T > \boldsymbol{0}$ of the filter algebraic Riccati equation (ARE), where

$$\boldsymbol{Y}\boldsymbol{A}^T + \boldsymbol{A}\boldsymbol{Y} - \boldsymbol{Y}\boldsymbol{C}^T\boldsymbol{V}^{-1}\boldsymbol{C}\boldsymbol{Y} + \boldsymbol{W} = \boldsymbol{0}. \tag{3.14}$$

The optimal state feedback gain

$$\boldsymbol{K_r} = \boldsymbol{R}^{-1}\boldsymbol{B}^T\boldsymbol{P} \tag{3.15}$$

is obtained with the solution $\boldsymbol{P} = \boldsymbol{P}^T > \boldsymbol{0}$ of the controller ARE

$$\boldsymbol{A}^T\boldsymbol{P} + \boldsymbol{P}\boldsymbol{A} - \boldsymbol{P}\boldsymbol{B}\boldsymbol{R}^{-1}\boldsymbol{B}^T\boldsymbol{P} + \boldsymbol{Q} = \boldsymbol{0}. \tag{3.16}$$

In the following, Q is defined by an output-weighted LQG design onset. Note that

$$\boldsymbol{y}^T\mathrm{I}\boldsymbol{y} = \boldsymbol{x}^T\underbrace{\boldsymbol{C}^T\boldsymbol{C}}_{\boldsymbol{Q}}\boldsymbol{x} \tag{3.17}$$

holds. For more details on LQG control see [29], [3], or [40].

Using the similarity transformation (as in Sec.2.2), any structural model can be diagonalized, and diagonal (modal) weighting matrices $\boldsymbol{Q}$ and $\boldsymbol{R}$ can be used. Since mode weights are already incorporated into the model, the $\boldsymbol{Q}$ matrix can be defined as unity matrix $\boldsymbol{Q} = \boldsymbol{I}_{[n\times n]}$ with dimension n, (see [10]). Other specifications can be easily implemented via an additional weighting.

In the case of comparing different actuators $j = 1, 2, ..|A|$ with a fixed set of outputs (sensor set S), comparability of the closed loops can be obtained by prescribing an identical controller $\mathcal{H}_2$ norm (see Eqn.3.4) $\|\boldsymbol{G}_r\|_2 = K$ for all design configurations. In this case, the controller $\mathcal{H}_2$ norm reflects the average gain (energy requirement) available for control.

The cost matrix $\boldsymbol{R}$ is defined as

$$\boldsymbol{R} = \alpha \cdot \boldsymbol{I}_{[r\times r]} \tag{3.18}$$

(whereas $\boldsymbol{I}_{[r\times r]}$ denotes an identity matrix with dimensions $r \times r$). The parameter α is adapted such that the final controller is essentially identical (to within a predefined

tolerance) in its energy requirement to controllers of the other selection configurations. The estimation of the factor α by *log-log* interpolation via the target $\mathcal{H}_2$ norm is computationally efficient, see Fig.3.4. The procedure of designing a fixed-norm controller is depicted in Fig.3.3 and is repeated for each actuator.

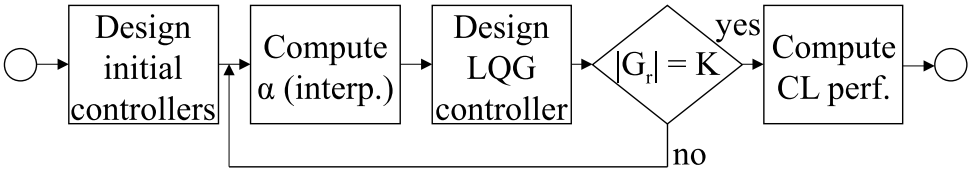

Figure 3.3: Control design steps for each actuator/sensor

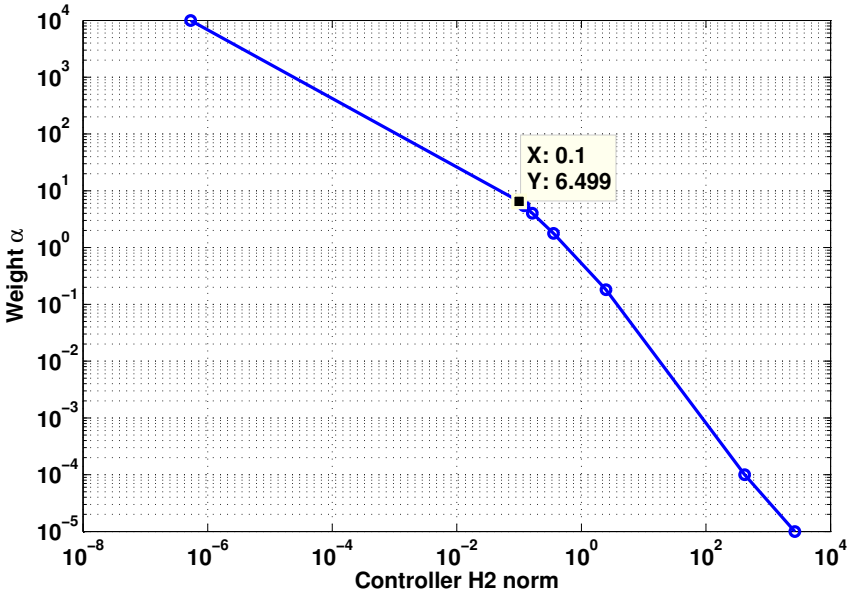

Figure 3.4: Estimation of the factor α by *log-log-interpolation*

It is obvious that the relationship between the controller $\mathcal{H}_2$ norm and the design weight α is close to linearity in a log-log scale, so using a linear interpolation in the log-log domain to determine the next value of α is computationally efficient.

It is not sought to design controllers with high authority because absolute performance is not of primary importance, but rather relative performance is evaluated.

One condition to ensure comparability is that none of the designed controllers change the system eigenfrequencies significantly. This can be verified by the evaluation of the singular values of the open and closed loop systems. Generally it is possible to find a broad range of target controller $\mathcal{H}_2$ norms which fulfil this require-

ment.

The closed-loop relative attenuation performance index $\mathrm{PI}_{\mathrm{cl}}$ is then defined using open and closed loop norms of the plant, in this case it is chosen as:

$$\mathrm{PI}_{\mathrm{cl}} = 1 - \frac{\|\boldsymbol{G}_{\mathrm{cl}}\|_2}{\|\boldsymbol{G}_{\mathrm{ol}}\|_2} \tag{3.19}$$

where $\boldsymbol{G}_{\mathrm{cl}}$ stands for $\mathcal{H}_2$ norm of the closed loop system using currently investigated input j and constant set S of outputs, and $\boldsymbol{G}_{\mathrm{ol}}$ represents the $\mathcal{H}_2$ norm of the open loop system actuated by all actuator candidates and the same fixed output set S. The quantity $\mathrm{PI}_{\mathrm{cl}}$ equals 1 for perfect attenuation and 0 for none (open loop behaviour).

An implementation of the proposed criterion is suggested in the following. A system with $j = 1, 2, ..|A|$ inputs and a fixed set of outputs S is considered.

INITIALIZATION

$*$ initialize weighting factor α

$*$ set $\boldsymbol{gap} = \infty$

$*$ set $\boldsymbol{u_{tolerance}}$ sufficiently small, e.g. 10^{-4}

$*$ define $\boldsymbol{\mathcal{H}_{2target}}$ - prescribed $\mathcal{H}_2$ norm of the final closed loop valid for all j

$*$ compute $\boldsymbol{OL_{all}}$ fully actuated open loop $\mathcal{H}_2$ norm, using all I/Os ($\boldsymbol{D}$=$\boldsymbol{0}$)

MAIN PROGRAM

for j=1 to A

$*$ design an LQG closed loop using α

$*$ compute loop's $\mathcal{H}_2$ norm and write it into $\boldsymbol{\mathcal{H}_{2normsvector}}$

While $|\boldsymbol{gap}| > \boldsymbol{u_{tolerance}}$

$*$ $\boldsymbol{\alpha_{new}}$ = interpolate ($\boldsymbol{\mathcal{H}_{2normsvector}}$, $\boldsymbol{\alpha}$, $\boldsymbol{\mathcal{H}_{2target}}$)

$*$ extend $\boldsymbol{\alpha}$ as follows: $\boldsymbol{\alpha} = [\boldsymbol{\alpha}; \boldsymbol{\alpha_{new}}]$

$*$ design the next closed loop using the last value in $\boldsymbol{\alpha}$

$*$ compute closed loop, it's $\mathcal{H}_2$ norm $\boldsymbol{CL, \mathcal{H}_{2normnew}, controller}_j$

$*$ $\boldsymbol{\mathcal{H}_{2normsvector}} = [\boldsymbol{\mathcal{H}_{2normsvector}, \mathcal{H}_{2normnew}}]$

$*$ $\boldsymbol{gap}$ = subtraction of latest elements of $\boldsymbol{\mathcal{H}_{2normsvector}}$ - $\boldsymbol{\mathcal{H}_{2target}}$

$*$ $\boldsymbol{system}_j$ = LFT [$\boldsymbol{OL_{all}}$, $\boldsymbol{controller}_j$]

$*$ performance index of j^{th}*actuator* :$\boldsymbol{PI}_{cl}(j) = \dfrac{\boldsymbol{system}_j}{\boldsymbol{OL_{all}}}$

end

According to [42], closed-loop I/O selection methods might not be suitable for large candidate sets due to high computational requirements. However, the present approach proved efficient and fast in implementation and has been successfully tested on problems with hundreds of I/Os.

The proposed method enables deeper insight into the system's closed loop dynamics. Frequency and saturation limits can be effectively introduced in time domain simulations. Careful choice of the target controller $\mathcal{H}_2$ norm can give additional system insight, for example by considering finite control energy (as opposed to Grammian-based open loop methods).

Also, non-linear systems or effects can be considered by extension of the proposed method. Since the LQ design is based on linearized systems, a grid of operating points has to be investigated in case of strong non-linearities.

It is useful for engineering applications to set the actuation effort by prescribing the controller $\mathcal{H}_2$ norm. For the case of sensor selection, it is advised to prescribe a transfer norm from system excitation to the selected sensor(s) and through the controller to ensure comparability.

3.3 Comparison of Method B and Method C - two LQ-based I/O selection methods

In this section, the Method B is compared with another I/O LQ-based selection criterion given in [4] which is denoted as Method C within this work. The methods characteristics are outlined and their applicability to an I/O selection problem in the well-known framework of LQG control is discussed.

Properties relevant for application are compared. Their usability is demonstrated at the input selection task for a simple flexible beam structure in hinged-hinged configuration. Results are given in Sec.4.3

The method B partially enumerates the candidate set and solves small LQG subproblems. It utilizes the LQG formalism and efficient tuning parameter search to design tuned LQG control loops for each candidate I/O set. This onset yields a highly flexible algorithm which is efficient for selecting single I/Os in problems with a high number of candidates. A normalized performance index can be formulated which reflects the efficiency of actuation / measurement. A technique to carry out this method in the form of a sensitivity analysis is discussed in [20] as well as in

Sec.3.2. This approach is of low computational complexity, but cannot guarantee global optimality in the multi-input (-output) case. Numeric results for the bending beam problem nevertheless show the efficiency of the set of selected inputs.

The Method C (see [4]) in contrast, takes a global optimization approach: an actuator (sensor) cost minimization problem is formulated and solved, whereby constraints related to preserving closed-loop stability and performance requirements are obeyed. The resulting Linear Matrix Inequalities (LMI) problem requires considerably higher numerical effort to solve, but a globally optimal solution to this problem can be obtained. The onset naturally yields a set of selected outputs (inputs) but is restricted to small or medium candidate sets. Numeric results show that this criterion yields strong discrimination between selected and disregarded candidates.

The Method C formulates the I/O selection problem as a cost minimization problem, based on several results related to LQG control (see 3.2). Thereby, in the input selection case, the diagonal entries of the matrix $\boldsymbol{R} = \mathrm{diag}(r_j)$, $j = 1, \ldots, r$ become decision variables. The idea is, under constraints guaranteeing a minimum degree of performance, to maximize these control cost coefficients (minimize their inverses) which results in a reduction of the utilized inputs to the essential ones for performance. The dual case of output selection can be viewed as maximization of the measurement noise covariance under given performance constraints.

Two aspects of performance constraints have been proposed in [4]: the so-called time-averaged performance index,

$$\sigma = \lim_{\substack{t_0 \to -\infty \\ t_1 \to \infty}} \frac{1}{t_1 - t_0} \mathrm{E} \left\{ \int_{t_0}^{t_1} \left(\boldsymbol{x}^T \boldsymbol{Q} \boldsymbol{x} + \boldsymbol{u}^T \boldsymbol{R} \boldsymbol{u} \right) \mathrm{d}t \right\} \tag{3.20}$$

$$= \mathrm{trace} \left(\boldsymbol{S}\boldsymbol{Q} + \boldsymbol{P}\boldsymbol{L}^T \boldsymbol{V} \boldsymbol{L} \right), \tag{3.21}$$

where $\boldsymbol{S}$, $\boldsymbol{P}$ are the solutions of the filter and regulator AREs, respectively, can be bounded above by the selection method. Moreover, the main diagonal elements p_{ii} of $\boldsymbol{P}$ can also be bounded, related to limiting the resulting state feedback gain magnitude. A linear objective is defined,

$$\mathrm{minimize}(\boldsymbol{\rho}^T \boldsymbol{z}), \tag{3.22}$$

where $\boldsymbol{\rho}$ are cost weights per input candidate and $\boldsymbol{z} = [z_1, \ldots, z_r]^T = [r_1^{-1}, \ldots, r_r^{-1}]^T$ are the inverse diagonal entries of $\boldsymbol{R}$. Written as Linear Matrix Inequalities (LMIs), the constraints are as follows:

Symmetric, positive-definite auxiliary matrix variables $\boldsymbol{P}, \boldsymbol{D}$ are introduced:

$$\boldsymbol{R}^{-1} = \operatorname{diag}(z_1, \ldots, z_r) > \mathbf{0} \tag{3.23}$$

$$\begin{bmatrix} \boldsymbol{P}^{-1} & \boldsymbol{I} \\ \boldsymbol{I} & \boldsymbol{D} \end{bmatrix} > \mathbf{0} \tag{3.24}$$

Next, the LMI

$$\begin{bmatrix} -\boldsymbol{P}^{-1}\boldsymbol{A}^T - \boldsymbol{A}\boldsymbol{P}^{-1} + \boldsymbol{B}\boldsymbol{R}^{-1}\boldsymbol{B}^T & \boldsymbol{P}^{-1} \\ \boldsymbol{P}^{-1} & \boldsymbol{Q}^{-1} \end{bmatrix} > \mathbf{0} \tag{3.25}$$

ensures that $\boldsymbol{P}$ is a stabilizing Riccati matrix of the LQR design problem, and the constraints

$$p_{ii}^* - \mathbf{e}_i^T \boldsymbol{D} \mathbf{e}_i > 0 \tag{3.26}$$

$$\sigma_\mu^* - \sum_n \boldsymbol{\mu}_i^T \boldsymbol{D} \boldsymbol{\mu}_i > 0 \tag{3.27}$$

allow to limit the deterioration of $\overline{\sigma}$ in (3.20) and limits feedback gain magnitude. The scalar σ_μ^* and vectors $\boldsymbol{\mu}_i$ are retrieved from a decomposition of the full LQG solution (with all input candidates active).

To this end, it can be stated that this method provides a global onset to the selection problem, but also requires to solve the LQG problem for the entire candidate set beforehand. Moreover, the stated LMI form generates a large optimization problem if the number of states or selection candidates grow large and is therefore limited to small- and medium-sized candidate sets. The basic properties of the discussed I/O selection methods are listed in Table 3.1. Method B uses several less complex LQG designs for each actuator separately while Method C is based on one large LMI problem including the whole candidate set of inputs. Implementation effort and also runtime is significantly higher. This method handles the I/O selection problem globally and yields globally optimal results, whereas Method B treats the multi-input selection problem in a greedy and thus sub-optimal manner. However, the observed difference in final quality is very small.

Table 3.1: Methods comparison

Property	**Method B**	**Method C**
Onset	SIMO/MISO enumeration, many small LQG designs	1 large LMI, 1-shot solution
Comp. complexity	[ARE $n \times n$] $\times\, r \times \log \frac{1}{tol} \rightarrow \mathcal{O}(n^3 r)$ (efficient)	$\mathcal{O}(r + n^2)$ LMI variables, LMI dim. $(r + 6n) \times (r + 6n)$ $\rightarrow \mathcal{O}(n^6, r^4)$ (expensive)
Implementation effort	ARE/LQG design, lightweight algorithm	LMI solver
Characteristics	aggregated criterion, artificial $\boldsymbol{R}$, sensitivity analysis	extremely discriminating criterion
Scope	local: single-actuator capability global: by partial/full enumeration	global: proposes set of actuators to use
Robustification	multi model, other PIs easily computable, flexible	must be represented in LQG/ARE/LMI form, restrictive

3.4 Method D - Robust I/O selection strategy for parameter depending systems

In many technical disciplines, the behavior of studied dynamical systems is strongly dependent on plant parameters. Especially in control applications varying plant parameters pose a challenge for standard design methods. If these parameters are slowly changing in operation compared to the relevant system dynamics, a significant reduction in complexity can be achieved by approximating a continuously parameter-dependent plant by a set of plants which have fixed parameter values valid only in the neighborhood of suitable operating points. This handling is demonstrated by Fig.3.5.

Numerous robust feedback control techniques are available to determine an optimal control law, which has to ensure adequate stability and sufficient performance in all operating points. A comprehensive robust control design task, as outlined in standard textbooks [40] and [47], necessarily includes all design stages - from system analysis, the selection of optimal inputs and outputs, the formulation of the control design problem, the actual control law synthesis, and finally its validation. Crucial

factors to achieve high overall control performance are the precision of modelling, an appropriate and efficient uncertainty formulation, and the use of effective design methods. This text focuses on the initial part of this process - system analysis and the selection of control inputs and measurements to ensure effective and efficient control for systems with varying parameter.

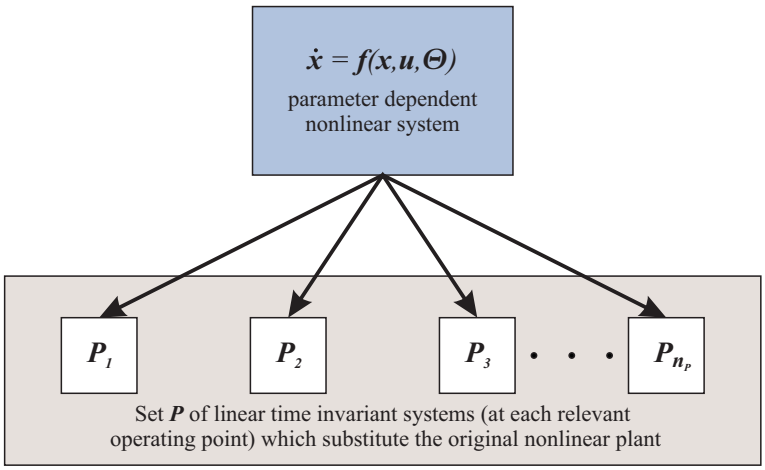

Figure 3.5: Substitution of one parameter depending system by a set of time invariant systems

For multi-input multi-output (MIMO) flexible structure systems, the achievement of desired control goals is strongly affected by the decision which measurements are chosen to be supplied to the controller to manipulate the given plant inputs. The input/output (I/O) selection task is crucial in the context of robust control because it affects the achievable robust performance of a subsequently designed controller. Considering the plant variation already in the I/O selection step yields optimal prerequisites for a good control performance, it can simplify the control design task and being closely related to system analysis, yield valuable system and design information.

Most of the available methods treat the I/O selection problem only for one nominal model. However, if parameter dependency of the plant dynamics exists, a more comprehensive approach is needed, which considers the system dynamics along all relevant operating points and by investigating of all individual I/O transfer function properties separately yields to a minimal and efficient set of I/O combinations for which a robustly performing controller may exist. Reasons for a limited I/O set are control system complexity constraints and constraints on the cost of operating and maintenance.

The I/O selection process of a highly complex dynamical system with hundreds

of modelled inputs and outputs based on a candidate by candidate feasibility check can lead to a combinatorial problem, where the number of I/O combinations grows quickly with the number of considered I/Os. Due to this fact, a systematic and efficient procedure must be found. Therefore, the main contribution of the presented method is an I/O selection strategy which treats the discussed problem in a fully automated and computational efficient way even for large systems with numerous I/O candidates.

In the following, the fundamentals of the proposed I/O selection technique are explained. The functionality of this method is validated by application to a simple flexible beam structure in Sec.4.4 and to a large passenger blended wing-body (BWB) concept aircraft in Sec.5.5.
This work is based on [21] presented on the 10^{th} International Conference on Motion and Vibration Control in Tokyo, Japan and extends the results therein. Moreover, presented technique has been submitted to the Journal of System Design and Dynamics (JSDD) and published by Japan Society of Mechanical Engineers (JSME) in August 2011 (see [22]).

Assume a general parameter-dependent dynamic plant which is given as

$$\begin{aligned} \dot{\boldsymbol{x}} &= \boldsymbol{f}(\boldsymbol{x}, \boldsymbol{u}, \boldsymbol{\theta}) \\ \boldsymbol{y} &= \boldsymbol{g}(\boldsymbol{x}, \boldsymbol{u}, \boldsymbol{\theta}), \end{aligned} \tag{3.28}$$

where $\boldsymbol{x}$, $\boldsymbol{u}$, and $\boldsymbol{\theta}$ are the state, input, and parameter vectors, respectively. If the functions $\boldsymbol{f}$ and $\boldsymbol{g}$ are significantly dependent on $\boldsymbol{\theta}$, but at the same time these parameters vary slowly compared to the plant dynamics in $\boldsymbol{x}$, the nonlinear plant (3.28) can be represented by a set $\boldsymbol{\mathcal{P}} = \{\boldsymbol{P}_i : i \in I_{\mathcal{P}} = \{1, \ldots, n_{\mathrm{P}}\}\}$ of linearized time-invariant (LTI) MIMO systems $\boldsymbol{P}_i$ with n_{o} outputs and n_{i} inputs, each associated to an equilibrium operating point parameterized by the set of parameter values $\boldsymbol{\theta}_i$. In transfer function notation, each LTI plant $\boldsymbol{P}_i$ is represented as an $n_{\mathrm{o}} \times n_{\mathrm{i}}$ transfer function matrix $\boldsymbol{G}_i(s) : C \to C^{n_{\mathrm{o}} \times n_{\mathrm{i}}}$:

$$\boldsymbol{G}_i(s) = \begin{bmatrix} G_{i,1,1}(s) & \ldots & G_{i,1,n_{\mathrm{i}}}(s) \\ \vdots & & \vdots \\ G_{i,n_{\mathrm{o}},1}(s) & \ldots & G_{i,n_{\mathrm{o}},n_{\mathrm{i}}}(s) \end{bmatrix}. \tag{3.29}$$

For $s = \mathrm{i}\omega$, $\omega \in R$, each transfer function $G_{i,j,k}(\mathrm{i}\omega)$ represents the complex

frequency response of plant i from input k to output j at frequency ω. Its magnitude $m_{i,j,k}(\omega) : R \to R^+$ and phase $\varphi_{i,j,k}(\omega) : R \to R$ are defined implicitly via [32]

$$G_{i,j,k}(\mathrm{i}\omega) \triangleq m_{i,j,k}(\omega)\mathrm{e}^{\mathrm{i}\varphi_{i,j,k}(\omega)} = \Re(G_{i,j,k}(\mathrm{i}\omega)) + \mathrm{i}\Im(G_{i,j,k}(\mathrm{i}\omega)), \tag{3.30}$$

where $\Re(\cdot)$ and $\Im(\cdot)$ denote the real and imaginary parts, respectively. The magnitude and phase can in turn be computed by

$$m_{i,j,k}(\omega) = |G_{i,j,k}(\mathrm{i}\omega)| = \sqrt{(\Re(G_{i,j,k}(\mathrm{i}\omega)))^2 + (\Im(G_{i,j,k}(\mathrm{i}\omega)))^2}, \tag{3.31}$$

$$\varphi_{i,j,k}(\omega) = \frac{1}{\mathrm{i}} \arg(G_{i,j,k}(\mathrm{i}\omega)) = \arctan\left(\frac{\Im(G_{i,j,k}(\mathrm{i}\omega))}{\Re(G_{i,j,k}(\mathrm{i}\omega))}\right) + n\pi \qquad n \in Z, \tag{3.32}$$

up to integer multiples of π. This offset can be determined by exploiting the smoothness of G as formulated in the following lemma:

Lemma 1 *Let*

$$G(s) = \frac{\prod_{\mu=1}^{m}(s - q_\mu)}{\prod_{\nu=1}^{n}(s - p_\nu)} = \frac{B(s)}{A(s)} \tag{3.33}$$

a real-rational, proper transfer function (zeros q_μ, poles p_ν, $m \leq n$) which is both analytic and nonzero along $s = \mathrm{i}\omega \ \forall \omega \in R$ (i.e. no poles or zeros of G lie on the imaginary axis, $\Re(q_\mu) \neq 0$, $\Re(p_\nu) \neq 0$). Then the following statements are true:

- *$G(\mathrm{i}\omega)$ is continuously differentiable.*
- *$G(\mathrm{i}\omega)$, $m(\omega)$, and $\varphi(\omega)$ are all locally Lipschitz continuous for all $\omega \in (-\infty; \infty)$:*

$$\exists K_1 \in R^+, 0 < K_1 < \infty : |G(\mathrm{i}(\omega + \delta\omega)) - G(\mathrm{i}\omega)| \leq K_1|\delta\omega| \tag{3.34}$$

$$\exists K_2 \in R^+, 0 < K_2 < \infty : |m(\omega + \delta\omega) - m(\omega)| \leq K_2|\delta\omega| \tag{3.35}$$

$$\exists K_3 \in R^+, 0 < K_3 < \infty : |\varphi(\omega + \delta\omega) - \varphi(\omega)| \leq K_3|\delta\omega|. \tag{3.36}$$

Proof: Local Lipschitz continuity of a function $y = f(x)$ with $f : X \to Y$, $x \in X$, $y \in Y$ is guaranteed iff for every $x \in X$ there exists a neighborhood $U \subseteq X$ in which the derivative of $f : U \to Y$ remains bounded: $\left|\frac{\mathrm{d}f}{\mathrm{d}x}\right| : U \to R^+, \left|\frac{\mathrm{d}f}{\mathrm{d}x}\right| \leq K < \infty$. This is fulfilled for $G(\mathrm{i}\omega)$ in Lemma 1 because its derivative is an analytic real-rational function which is bounded for $\omega \in (-\infty; \infty)$:

$$\frac{\mathrm{d}G(\mathrm{i}\omega)}{\mathrm{d}\omega} = \frac{A(\mathrm{i}\omega)\frac{\mathrm{d}B(\mathrm{i}\omega)}{\mathrm{d}\omega} - \frac{A(\mathrm{i}\omega)}{\mathrm{d}\omega}B(\mathrm{i}\omega)}{(A(\mathrm{i}\omega))^2} \tag{3.37}$$

where $A(\mathrm{i}\omega) \neq 0$, $(A(\mathrm{i}\omega))^2 \neq 0$, and since the numerator is a polynomial in ω, there always exists, for any chosen finite ω, a positive and finite constant K_1 such that (3.34) is fulfilled. This also directly proves (3.35) as it is a metric on (3.34). To prove (3.36), note that (3.33) can be written for $s = \mathrm{i}\omega$ as

$$G(\mathrm{i}\omega) = \underbrace{\frac{\prod_{\mu=1}^{m} |\mathrm{i}\omega - q_\mu|}{\prod_{\nu=1}^{n} |\mathrm{i}\omega - p_\nu|}}_{m(\omega)} \underbrace{\mathrm{e}^{\mathrm{i}\left(\sum_{\mu=1}^{m} \arg(\mathrm{i}\omega - q_\mu) - \sum_{\nu=1}^{n} \arg(\mathrm{i}\omega - p_\nu)\right)}}_{\mathrm{e}^{\mathrm{i}\varphi(omega)}}. \tag{3.38}$$

For the stable case, the phase contributions of each single pole and zero result from the principal branch of the arctan function:

$$\arg(\mathrm{i}\omega - q_\mu) = \arctan\left(\frac{\omega - \Im(q_\mu)}{-\Re(q_\mu)}\right), \quad \arg(\mathrm{i}\omega - p_\nu) = \arctan\left(\frac{\omega - \Im(p_\nu)}{-\Re(p_\nu)}\right), \tag{3.39}$$

and its derivative yields

$$\frac{\mathrm{d}\varphi}{\mathrm{d}\omega}(\omega) = \sum_{\mu=1}^{m} \frac{1}{1 + (\arg(\mathrm{i}\omega - q_\mu))^2} \frac{1}{-\Re(q_\mu)} - \sum_{\nu=1}^{n} \frac{1}{1 + (\arg(\mathrm{i}\omega - p_\nu))^2} \frac{1}{-\Re(p_\nu)} \tag{3.40}$$

which can be bounded by

$$-K_3 \leq \frac{\mathrm{d}\varphi}{\mathrm{d}\omega}(\omega) \leq K_3 \qquad K_3 = \sum_{\mu=1}^{m} \left|\frac{1}{\Re(q_\mu)}\right| + \sum_{\nu=1}^{n} \left|\frac{1}{\Re(p_\nu)}\right|. \tag{3.41}$$

□

Remark: It is evident that, starting from $\omega = 0$, the phase evolution can be traced uniquely over sufficiently small frequency increments $\Delta\omega$. This justifies the standard numeric procedures for the so-called phase unwrapping.

The considered system possesses real and complex-conjugate (oscillatory) modes. Note that all transfer functions $G_{i,j,k}(\mathrm{i}\omega)$ for a fixed plant i share the same denominator polynomial $A(s)$ whose zeros comprise all modes of the system. In the following, the proposed selection methods focus on low-damped oscillatory modes (such as elastic modes of flexible structures). However, the remaining modes may reflect important parameter dependency and are therefore retained in the system description to account for these effects.

The proposed approach for selection of appropriate I/O candidates for robust controller design, considering a flexible MIMO structure, is presented in the following.

Starting from the initial I/O candidate set $\boldsymbol{\mathcal{S}}$ with a candidate defined as the ordered pair of input and output indices $\boldsymbol{s} = (j, k) \in \boldsymbol{\mathcal{S}}$, the proposed procedure involves a pre-processing and three consecutive selection steps, each applying its respective selection criterion on the remaining subset of candidate I/Os. Each criterion is a necessary condition which must be fulfilled by the specific I/O combination in order to pass the step, so the sets of remaining I/O candidates $\boldsymbol{\mathcal{S}}_r$, $r = 1, 2, 3$ after step r are typically much smaller subsets of $\boldsymbol{\mathcal{S}}$:

$$\boldsymbol{\mathcal{S}} \supseteq \boldsymbol{\mathcal{S}}_1 \supseteq \boldsymbol{\mathcal{S}}_2 \supseteq \boldsymbol{\mathcal{S}}_3 \tag{3.42}$$

The reduction of the number of I/O candidates after each step leads to both time and computational efficiency. The outcome of the presented technique is a comparatively small set $\boldsymbol{\mathcal{S}}_3$ of I/O combinations which are suitable for robust control design. The I/O selection procedure is illustrated in Fig. 3.6.

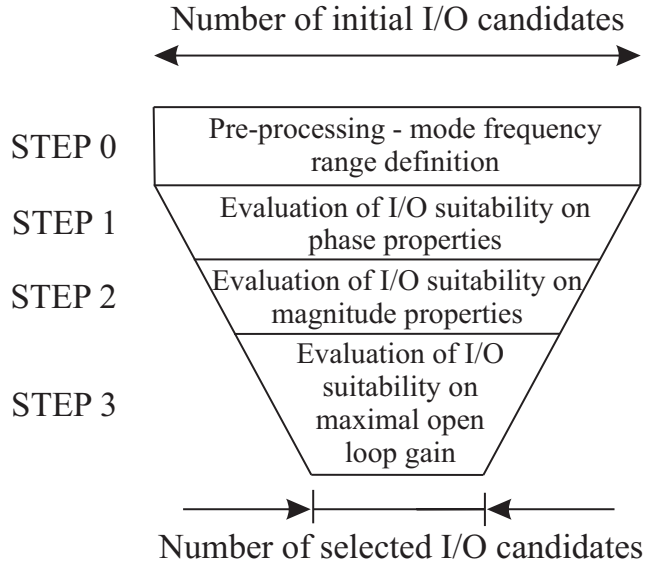

Figure 3.6: Graphical depiction of proposed I/O selection strategy

Step 0 - Preprocessing

The set of considered modes $l = 1, \ldots, n_{\text{modes}}$ and their peak frequency ranges $\Omega_l = \{\omega \in R : \underline{\omega} \leq \omega \leq \overline{\omega}\}$ (with boundary frequencies $\underline{\omega}, \overline{\omega} \in R$) are defined in the preprocessing step, also expert knowledge can be incorporated at this point. Only low-damped oscillatory modes are considered here. Moreover, it is assumed

that these modes are mutually separated over the frequency range ($\Omega_{l_1} \bigcap \Omega_{l_2} = \emptyset$ if $l_1 \neq l_2$) and that these ranges are known a priori. An automated procedure for the computation of the frequency ranges Ω_l is given by the following algorithm:

1. Compute the considered modes' eigenfrequencies of all plants
   $\omega_{i,l}$ ($i = 1, \ldots, n_{\mathrm{P}}$, $l = 1, \ldots, n_{\mathrm{modes}}$).
2. For each mode l find the minimal and maximal frequencies
   $$\underline{\omega}_l = \min_{i=1}^{n_{\mathrm{P}}} \omega_{i,l} \qquad \overline{\omega}_l = \max_{i=1}^{n_{\mathrm{P}}} \omega_{i,l}. \tag{3.43}$$
3. Define the frequency range $\Omega_l = [\underline{\omega}_l - \Delta\omega_l, \overline{\omega}_l + \Delta\omega_l]$ with a suitable value of $\Delta\omega_l > 0$ and verify that all intervals are disjoint.
   Remark: If the disjointness property is not fulfilled, user intervention is required to determine, specific to the application, which modes are relevant for the I/O selection task. Careful choice of $\Delta\omega_l$ allows to implement expert knowledge.

As a result, frequency ranges Ω_l covering the modes' frequency variations are defined. The fact that they are generally larger than the spread of the actual values found in the set of plants allows for magnitude and phase regularity checks in the neighbourhood of the modes, which leads to improved reliability of the automated selection algorithm.

For numeric computations, it is necessary to utilize discretized frequency grids that sample the intervals defined above:

$$\widetilde{\omega}_{l,q} \in \widetilde{\Omega}_l = \{\underline{\omega}_l - \Delta\omega_l, \ldots, \overline{\omega}_l + \Delta\omega\} \qquad q = 1, \ldots, n_\omega. \tag{3.44}$$

The frequency resolution required to meet a given accuracy in magnitude and phase statements is related to the bounds on the magnitude and phase derivatives, compare Lemma 1.

Step 1 - Maximum phase difference

The key idea of the first step is to eliminate those I/O combinations that cause a designed controller not to perform robustly. This is clearly the case if a controlled mode is subject to large phase variations in the utilized I/O channels (taken at a fixed frequency $\widetilde{\omega}_{l,q}$ over all plants $\boldsymbol{P}_i$). Note that a SISO controller that increases damping at a given mode in one plant excites the same mode in another plant if their phase

difference is more than $\frac{\pi}{2}$. Thus, starting from all modeled I/O combinations $\boldsymbol{s} = (j,k) \in \boldsymbol{\mathcal{S}}$, selection step 1 eliminates all I/O combinations whose phase variations $\Delta\varphi_{(j,k),l}$ over all plants $\boldsymbol{P}_i$ and modes l exceed a given threshold $\alpha \in \left(0; \frac{\pi}{2}\right)$:

$$\Delta\varphi_{(j,k),l} \leq \alpha \quad \forall l \in \{1, \ldots, n_{\text{modes}}\} \quad \ldots \quad (j,k) \text{ passes step 1}, (j,k) \in \boldsymbol{\mathcal{S}}_1 \tag{3.45}$$

$$\text{otherwise} \quad \ldots \quad (j,k) \text{ fails step 1}, (j,k) \notin \boldsymbol{\mathcal{S}}_1 \tag{3.46}$$

The maximum phase variation $\Delta\varphi_{(j,k),l}$ of a given I/O combination (j,k) and mode l is computed as

$$\Delta\varphi_{(j,k),l} = \min_{i_1 \in I_{\mathcal{P}}} \left\{ \max_{i_2 \in I_{\mathcal{P}}, i_1 \neq i_2} \left[\min_{n \in Z} \left(\max_{\widetilde{\omega}_{l,q} \in \widetilde{\Omega}_l} |\phi_{i_1,j,k}(\widetilde{\omega}_{l,q}) - \phi_{i_2,j,k}(\widetilde{\omega}_{l,q}) + 2n\pi| \right) \right] \right\}. \tag{3.47}$$

Thereby, the phases are shifted by integer multiples of 2π to yield the smallest maximal absolute value difference. Additionally, all-by-all plant combinations (i_1 can be considered as central or design plant index, i_2 as the compared plant's index) are scanned. After solving this combinatorially, the optimal value $\Delta\varphi_{(j,k),l}$ and the arguments i_1, i_2, n, and $\widetilde{\omega}_{l,q}$ can be extracted. In particular, $\boldsymbol{P}_{i_1}$ may be of interest as a potential design plant choice for subsequent control design. Note, however, that this criterion does not restrict this central plant to be the same across all modes of the investigation.

Figure 3.7 depicts transfer function and phase of two plants at their second eigenfrequency and illustrates the proposed criterion. Transfer functions and phases derived from I/O combination are shown for the example given in Sec. 4, Fig. 4.2.

I/O combinations eliminated in this first step are not subject to further investigation. Moreover, they are classified as unsuitable for robust control synthesis.

The maximal acceptable phase difference α can be set arbitrarily, which is an advantage of the proposed method and allows expert knowledge as well as specific requirements to be considered. While robust performance (in SISO control) is only possible for $\alpha \leq \frac{\pi}{2}$, a lower threshold value intends to emphasize robust performance requirements. Although it is not guaranteed that passed I/O combinations in $\boldsymbol{\mathcal{S}}_1$ lead to a successful robust control design, the worst candidates (that are not useful for robust performance objectives) are eliminated.

Step 2 - Modal energy transfer

Selection step 2 employs a further necessary criterion on the I/O combinations in $\boldsymbol{\mathcal{S}}_1$. A magnitude peak detection is carried out and those I/O combinations which

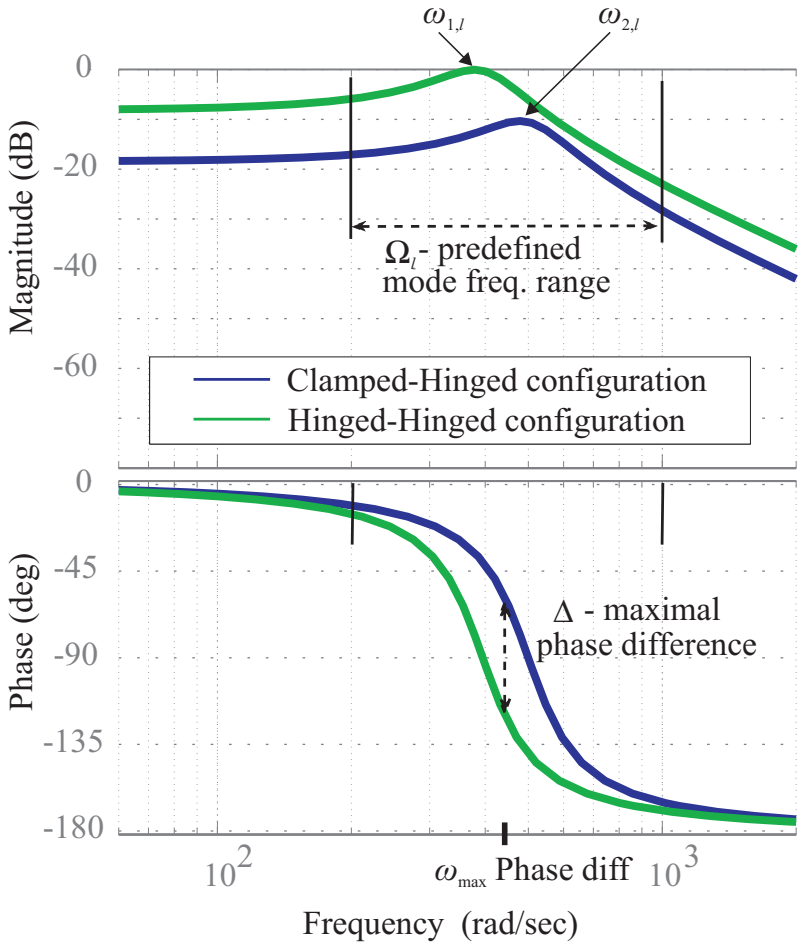

Figure 3.7: Bode plot of a mode l of two systems from input k to output j

show a pronounced resonance peak in the considered frequency range pass the step. This is a specific, heuristic criterion for control objectives associated to damping of low-damped oscillatory modes. If such peak is present, energy can be effectively transmitted through the system at this mode and through this I/O combination. In contrast, closely located zeros (modal nodes) reduce or eliminate the resonance peak, which is undesirable from both efficiency and robustness perspectives. With a chosen threshold $\beta_{dB} = 20\log_{10}(\beta) > 0$, the criterion is formulated for all $\boldsymbol{s} = (j,k) \in \boldsymbol{\mathcal{S}}_1$ as:

$$\left(\Delta m_{(j,k),l}\right)_{dB} \geq \beta_{dB} \;\forall l \in \{1,\ldots,n_{\text{modes}}\} \ldots (j,k) \text{ passes step 2}, (j,k) \in \boldsymbol{\mathcal{S}}_2 \quad (3.48)$$

$$\text{otherwise} \quad \ldots \quad (j,k) \text{ fails step 2}, (j,k) \notin \boldsymbol{\mathcal{S}}_2 \quad (3.49)$$

The peak height is measured in dB as the difference from the peak maximum to the maximum boundary magnitude value, whereby the minimum peak height over

all plants in $\boldsymbol{\mathcal{P}}$ is utilized:

$$\left(\Delta m_{(j,k),l}\right)_{dB} = \min_{i \in I_{\mathcal{P}}} \left\{ \max_{\widetilde{\omega}_{l,q} \in \widetilde{\Omega}_l} \left[m_{i,j,k,dB}(\widetilde{\omega}_{l,q}) - m_{i,j,k,l,dB,\mathrm{bnd}} \right] \right\} \tag{3.50}$$

with

$$m_{i,j,k,l,dB,\mathrm{bnd}} = \max([m_{i,j,k,dB}(\underline{\omega}_l - \Delta\omega_l), m_{i,j,k,dB}(\underline{\omega}_l + \Delta\omega_l)]) \tag{3.51}$$

as the maximum magnitude value at the boundaries of the frequency range $\widetilde{\Omega}_l$ of mode l. After evaluating the step 2 selection criterion in Eqn. (3.50), all selected I/O combinations $\boldsymbol{s} \in \boldsymbol{\mathcal{S}}_2$ are guaranteed to show a distinct peak with a minimum height of β_{dB} for every considered mode.

Step 3 - Maximum transfer gain

While step 1 and step 2 ensure that the selected I/O combinations fulfil qualitative requirements on phase and peak shape, step 3 evaluates the remaining I/O combinations $\boldsymbol{s} = (j,k) \in \boldsymbol{\mathcal{S}}_2$ quantitatively. Let $M_{(j,k,l)}$ be the peak magnitude of mode l (minimum over all plants) associated with I/O combination (with input k and output j) and δ_{dB} the required magnitude threshold to pass step 3, then for all $\boldsymbol{s} = (j,k) \in \boldsymbol{\mathcal{S}}_2$ the step 3 criterion is defined as:

$$M_{(j,k,l)} \geq \delta_{dB} \quad \forall l \in \{1, \ldots, n_{\mathrm{modes}}\} \quad \ldots \quad (j,k) \text{ passes step 3}, (j,k) \in \boldsymbol{\mathcal{S}}_3 \tag{3.52}$$

$$\text{otherwise} \quad \ldots \quad (j,k) \text{ fails step 3}, (j,k) \notin \boldsymbol{\mathcal{S}}_3. \tag{3.53}$$

with

$$M_{(j,k,l)} = \min_{i \in I_{\mathcal{P}}} \left\{ \max_{\widetilde{\omega}_{l,q} \in \widetilde{\Omega}_l} \left[m_{i,j,k,dB}(\widetilde{\omega}_{l,q}) - m_{i,j,k,l,dB,\mathrm{bnd}} \right] \right\}. \tag{3.54}$$

Note that when comparing different I/O combinations in their modal peak magnitudes, it is crucial that they are normalized to some common reference magnitudes [40], for example by the admissible input amplitudes and expected measurement dynamic ranges of the sensors.

Properties of Method D:

Note that the result of the proposed selection procedure is threefold:

- Each I/O combination $\boldsymbol{s} = (j,k) \in \boldsymbol{\mathcal{S}}_3$ fulfills all three criteria, so they are considered as suitable for robust control design.
- Candidates for phase-optimal central plants $\boldsymbol{P}_{i_1}$ can be extracted from step 1.
- The quantity $M_{(j,k,l)}$ for $\boldsymbol{s} = (j,k) \in \boldsymbol{\mathcal{S}}_3$ serves as a relative, quantitative, and mode-wise measure in the form of a selection index. Those I/O combinations with largest $M_{(j,k,l)}$ are expected to result in highest effectiveness and robustness in controlling of mode l.

Chapter 4

Demonstrative example - optimal I/O selection for simple flexible beam

The optimal I/O selection methods presented along Sec.3 have been applied to a simple flexible beam. Two different beam layouts are considered.
The Method A and Method B, respectively the Method C ([4]) deal with the beam set-up shown on Fig.4.1.

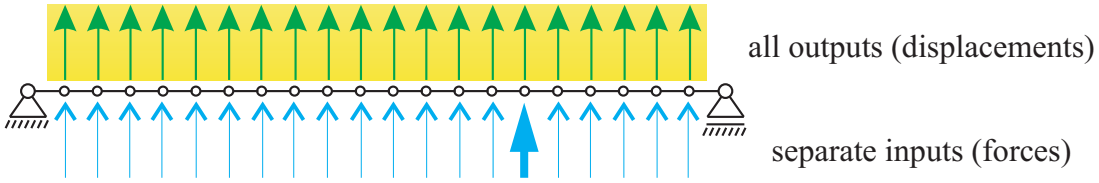

Figure 4.1: Transversal weakly damped Bernoulli beam in hinged/hinged configuration

In this case, a transversal Bernoulli beam dynamics in hinged-hinged configuration is considered. The model consists of 21 discretized elements. Only first three structural modes are modeled (see Sec.2.2). Input candidate set is represented by a transversal force at each node. Outputs are all transversal modal displacements. For more details on modelling see [10]. The goal is to find an appropriate I/Os to operate first three structural modes optimally. Outlined results validate the functionality of selection criteria presented in this thesis.

The Method D is applied to diverse beam configurations, hence the simultaneous consideration of different dynamics is possible. They are shown on Fig.4.2.

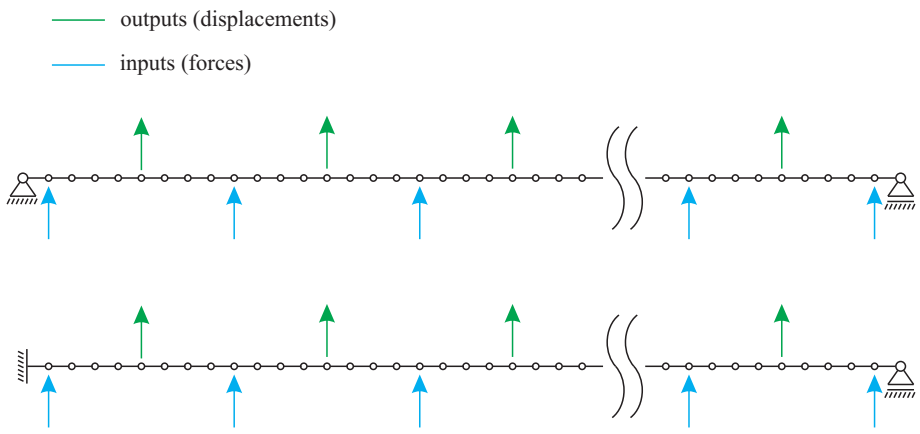

Figure 4.2: Beam setup (top: hinged-hinged configuration; bottom: clamped-hinged configuration)

In this case, the system model consists of $n_{\mathrm{el}} = 202$ identical FE elements of length $\Delta x = \frac{l}{n_{\mathrm{el}}}$ whereby only non-collocated actuating and measurement positions are examined. They are positioned alternately with constant spacing: $n_{\mathrm{i}} = 26$ inputs at $x_k = (8(k-1)+1)\Delta x$ and $n_{\mathrm{o}} = 25$ outputs at $x_j = (8(j-1)+5)\Delta x$ are available. The considered beam model is constructed from its analytic solution of its eigenvalue / eigenshape problem as stated in [39] (see also [27] and [26]). The vertical displacement of a beam $w(x,t)$ as shown in Fig. 4.11 as function of time $g(t)$ and spatial coordinate $f(x)$ can be written as:

$$w(x,t) = g(t)f(x), \tag{4.1}$$

where $g(t) = a\cos(\omega t - \epsilon)$, $f(x) = b_1\sin(\gamma x) + b_2\cos\gamma x + b_3\sinh(\gamma x) + b_4\cosh(\gamma x)$, and the coefficient vector is given by $[b_1, b_2, b_3, b_4]$. The boundary-value problem can be stated as

$$\boldsymbol{M}(\gamma l)\begin{bmatrix} b_1 \\ b_2 \\ b_3 \\ b_4 \end{bmatrix} = \begin{bmatrix} 0 \\ 0 \\ 0 \\ 0 \end{bmatrix}, \qquad |\boldsymbol{M}(\gamma l)| = 0, \tag{4.2}$$

where $\boldsymbol{M}$ is the (4×4) boundary conditions coefficient matrix for the general form of $f(x)$. For two given boundary conditions and the 2^{nd} mode, the coefficient vectors are:

- for the hinged-hinged case, $\gamma l = 2$, $\quad [b_1, b_2, b_3, b_4] = [1, 0, 0, 0]$,
- for the clamped-hinged case, $\gamma l = 7.07$, $\quad [b_1, b_2, b_3, b_4] = [1, 1, 1, 1]$.

The beam's state-space model of this 2^{nd} mode in modal form can be written as stated in [10]:

$$\dot{\boldsymbol{x}} = \begin{bmatrix} 0 & 1 \\ -\omega^2 & -2\zeta\omega \end{bmatrix} \boldsymbol{x} + \begin{bmatrix} 0 \\ \boldsymbol{f}(x_k) \end{bmatrix} \boldsymbol{u}, \quad \boldsymbol{y} = \begin{bmatrix} \boldsymbol{f}(x_j) & 0 \end{bmatrix} \boldsymbol{x} \tag{4.3}$$

where $\omega = \gamma^2 \sqrt{\frac{EI}{\rho A}}$ is the undamped eigenfrequency (Young's modulus E, moment of inertia I, density ρ, and cross-section area A, see [39]), ζ is the damping coefficient ($0 < \zeta \ll 1$), and $\boldsymbol{f}$ is the column vector function of the eigenshape function evaluated at the actuation / measurement locations (x_k, x_j, respectively). The robust I/O selection valid for both set-ups will be outlined.

4.1 Method A - I/O selection results

The optimal I/O selection results evaluated by the Method A ([10]) applied to the beam configuration depicted on Fig.4.1 are here given. Considering a simple flexible beam in hinged-hinged configuration with 20 input and output candidates, the best performing locations related to first three structural modes are selected. Visualization of $\boldsymbol{\Sigma}_{\text{act}}$ is depicted on Fig.4.3 where performance to I/O candidates in relation to individual structure modes is assigned. .

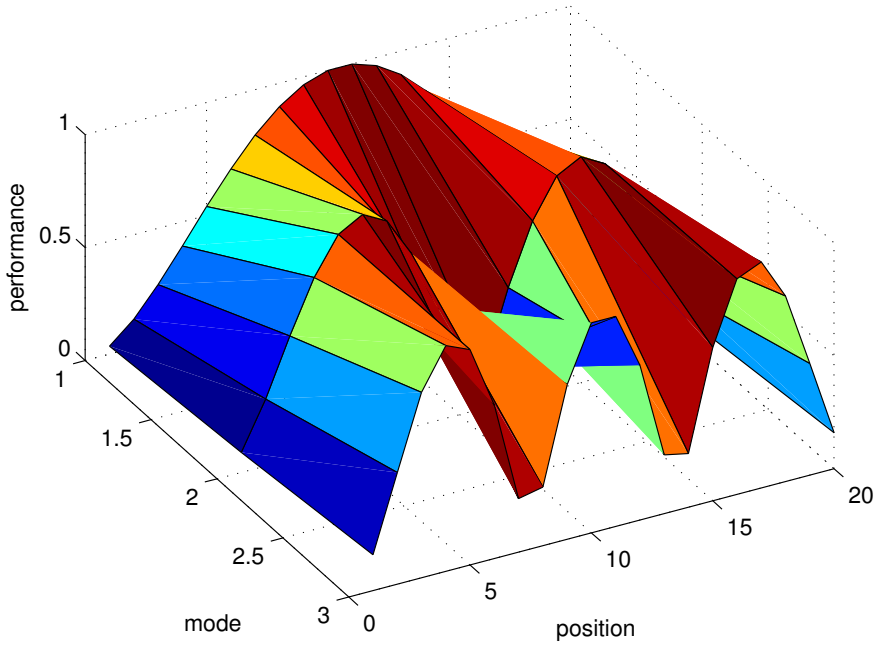

Figure 4.3: Performance matrix of considered beam structure

4.2 Method B - I/O selection results

A simple uniform flexible beam in a hinged-hinged configuration as in Fig.4.1 is here considered. Only the first three modes are investigated, no further system weighting has been done, the inputs are n transverse forces at the nodes, and the outputs are all nodal traversal displacements.

Fig.4.4 shows optimal I/O selections evaluated by Method B (see Sec.3.2) compared to the results computed by Method A (see. [10]) which is here employed as a reference I/O placement criterion. The results are scaled to a maximal value of 1, and show that globally both criteria yield similar results. However, minor differences do occur.

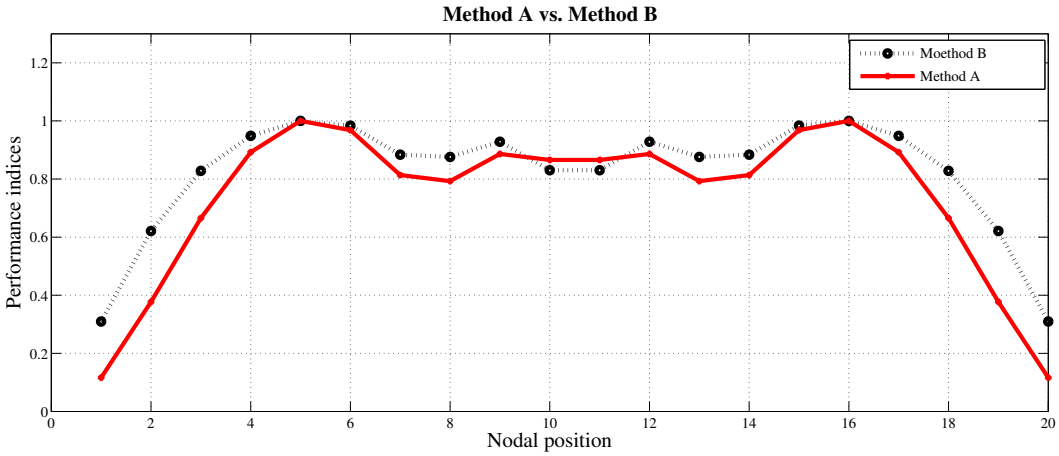

Figure 4.4: Method A vs. Method B - selected I/Os

As demonstrated above, Method B provides a reliable results for system with constant parameters in time. That means, before applying this I/O selection strategy it must be assumed, that the system dynamics is time invariant. If the system parameters are changing in the time, another type of I/O selection must be employed to ensure desired controllability and observability over whole operating range.

4.3 Method B and Method C - I/O selection results

In this text, optimal I/O selection results related to the beam configuration depicted on Fig.4.1 are discussed. They are evaluated by the Method B (Sec.3.2, [20]) and Method C ([4]), respectively.

Fig.4.5 shows the results of an input efficiency sensitivity analysis study (Method B) obtained for small control input magnitudes (high control cost). The outlined iterative design procedure has been carried out to retrieve a small controller $\mathcal{H}_2$ norm of 0.1 using only a single control input. The performance index varies smoothly with the input position and is an aggregated measure related to the mode shapes.

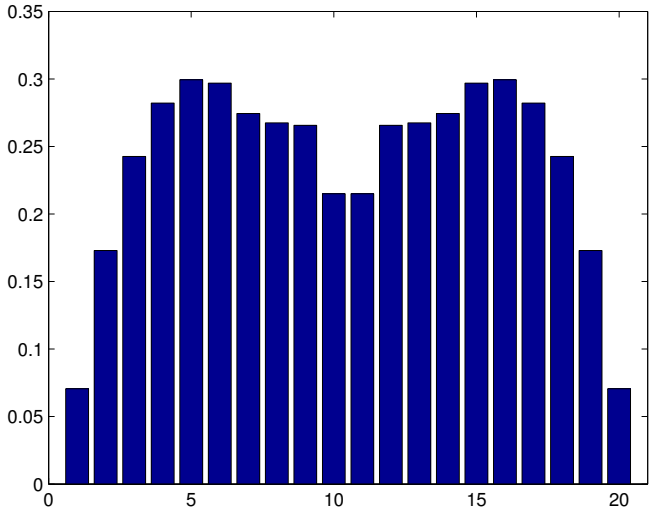

Figure 4.5: Method B - sensitivity analysis

Fig.4.6 shows sensitivity results (high control cost), however for a pair-wise selection of the inputs. The best input pair $(5, 16)$ is selected and chosen. Then, more input pairs are evaluated and added, whereby the LQG control design procedure always also utilizes the previously fixed inputs from earlier iterations. Fig. 4.7–4.9 illustrate these iterations in which the input pairs $(6, 15)$, $(4, 17)$, and $(9, 12)$ are added. Table 4.1 lists the results of each iteration and relevant performance quantities for two controller configurations: the low-authority K_{sens} with specified small $\mathcal{H}_2$ norm (which is the basis for the selection), and the controller K_{orig} resulting from the original LQG weightings with the input set found in that iteration.

Table 4.1: Method B - selected I/Os

Iter.	input set (new in **bold**)	$\|_{\text{sens}}\|_2$	$\text{PI}_{\text{cl}}(_{\text{sens}})$	$\overline{\sigma}(_{\text{sens}})$	$\|_{\text{orig}}\|_2$	$\text{PI}_{\text{cl}}(_{\text{orig}})$	$\overline{\sigma}(_{\text{orig}})$
1	(**5**,**16**)	0.1	0.337	49.93e-3	20.52	0.4999	8.33e-3
2	(5,**6**,**15**,16)	0.2	0.413	23.71e-3	91.13	0.5072	4.86e-3
3	(**4**,5,6,15,16,**17**)	0.4	0.458	14.92e-3	83.96	0.5074	4.80e-3
4	(4,5,6,**9**,**12**,15,16,17)	0.8	0.481	7.43e-3	61.44	0.5077	4.66e-3
ref.	(1,..,20)				54.68	0.5079	4.63e-3

Table 4.2 lists a comparison of the performance attainable by multi-input selections found by both methods. Here, for 6 symmetrically selected inputs, method C obtains the best results in terms of the $\mathcal{H}_2$ norm as well as in the time-averaged performance index $\overline{\sigma}$, but the selections found by method B are very close.

Table 4.2: Selected I/Os by the Method B and Method C

Method	input set	$\|\|_{\text{orig}}\|_2$	$\text{PI}_{\text{cl}}(_{\text{orig}})$	$\overline{\sigma}(_{\text{orig}})$
B (sens.)	(4,5,6,15,16,17)	83.96	0.5074	4.80e-3
B (sens.)	(4,5,6,9,12,15,16,17)	61.44	0.5077	4.66e-3
B (orig.)	(4,7,10,11,14,17)	61.40	0.5076	4.66e-3
C	(5,6,10,11,15,16)	61.22	0.5077	4.66e-3
ref.	(1,..,20)	54.68	0.5079	4.63e-3

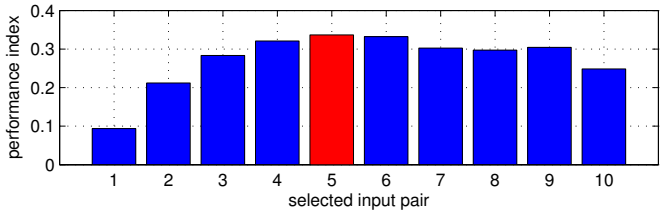

Figure 4.6: Method B, pairwise evaluation with high control cost, iteration 1

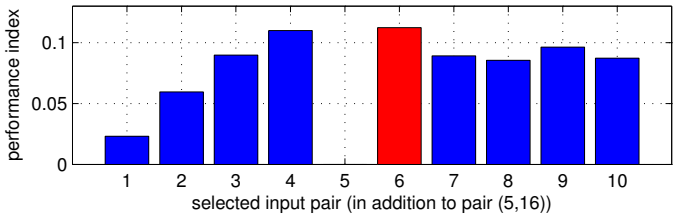

Figure 4.7: Method B, pairwise evaluation with high control cost, iteration 2

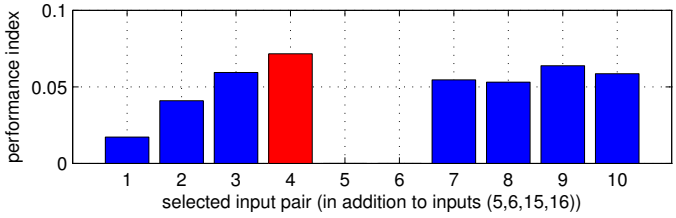

Figure 4.8: Method B, pairwise evaluation with high control cost, iteration 3

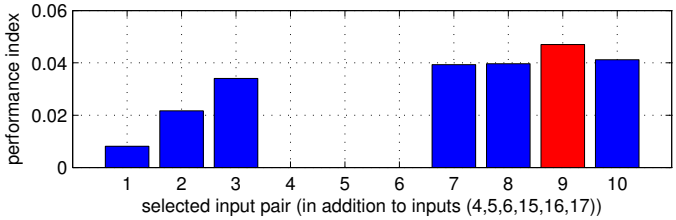

Figure 4.9: Method B, pairwise evaluation with high control cost, iteration 4

Fig. 4.10 shows the optimal solution of the Method C ([4]) in terms of the decision variable values (inverse control input cost). It is evident that this result is very discriminatory compared to the results of Method B. From Table 4.2 it is also evident that this method yields the best found selection set of 6 inputs. In turn, this method is significantly more complex both conceptionally as well as computationally.

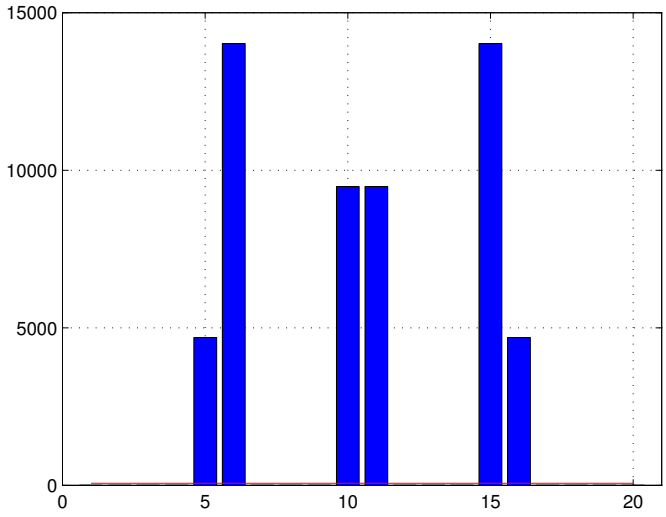

Figure 4.10: Method C - selected I/Os

4.4 Method D - I/O selection results

Here, the effectiveness of the Method D is demonstrated at a simple flexible beam in both clamped-hinged and hinged-hinged configurations as in Fig.4.2. These two set-ups represent system with varying parameter.

The aforementioned two differently supported beams constitute the set of plants $\boldsymbol{\mathcal{P}}$ with $n_{\mathrm{P}} = 2$. The I/O combinations suitable for robust control design with the goal to dampen the second structural mode have to be selected. Note that only the second structural mode is investigated in this example due to the brevity of the presentation.

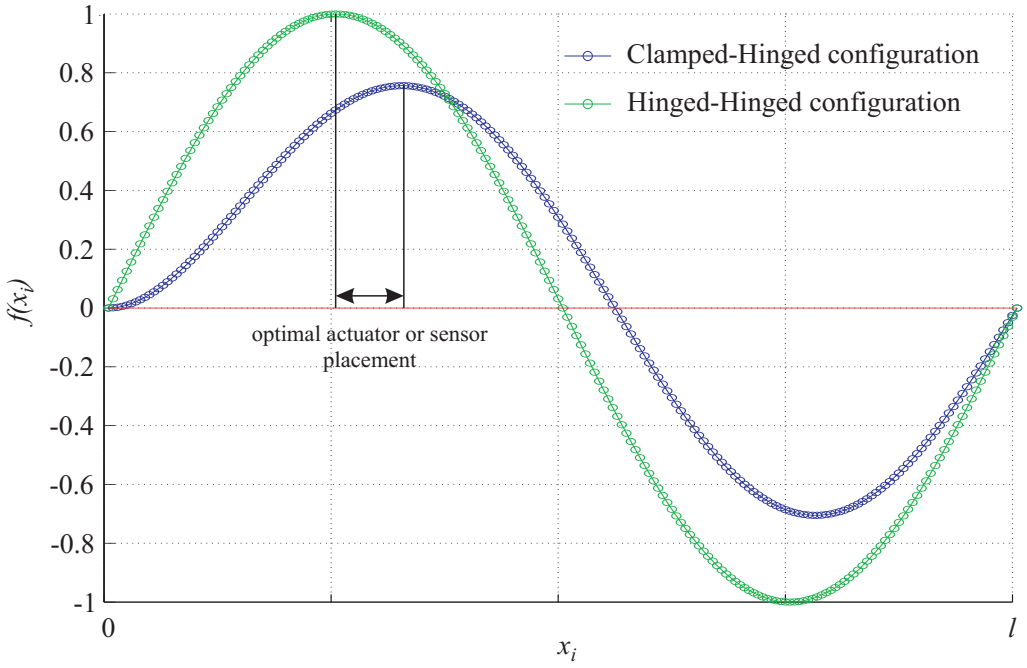

Figure 4.11: Mode shapes at second structural resonance

The proposed methodology yields an index value for each I/O combination $\boldsymbol{s} = (j, k)$ which refers to the predicted suitability of a certain I/O pair for robust controller synthesis with a predefined control goal. Fig. 4.12 shows selected I/O candidates which, according to the Method D, allow to design a robustly performing controller. Remaining candidates are assigned by colour to the step at which they have been eliminated. Asymmetries enter the solution because of the asymetric 2^{nd} mode shape of the clamped-hinged beam configuration. Hence, the best suited positions for inputs and outputs in the context of robust control are collocated at one third of the beam's length. These positions show the highest ability to robustly transfer energy into and from the system.

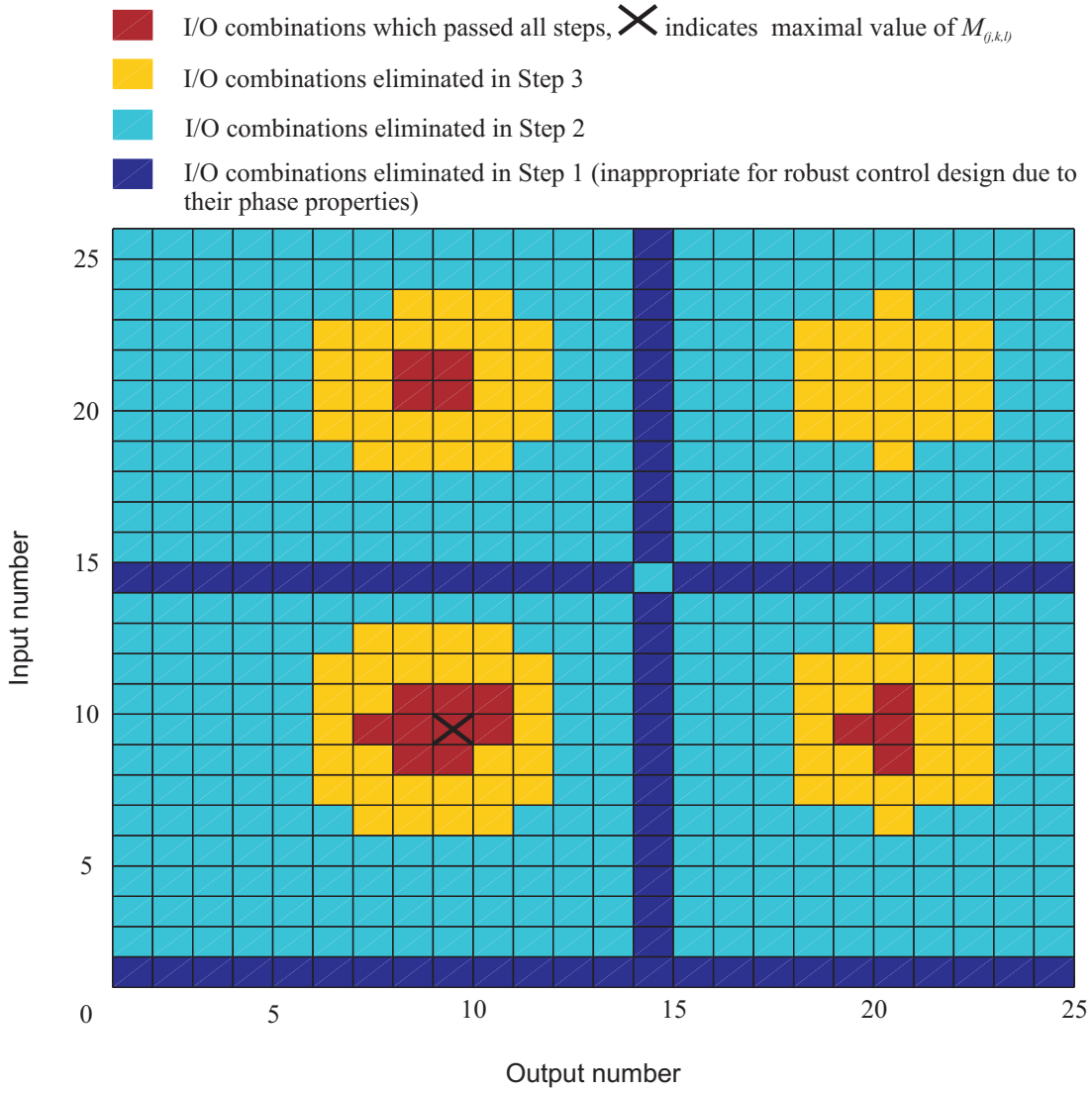

Figure 4.12: Eliminated and preferred I/O combinations by Method D

Chapter 5

A case study - the blended wing body aircraft configuration

In this text, after a brief overview on airframe evolution, two specific blended wing body models are introduced. The aim of this section is to show applicability of proposed criteria given in Sec.3 to a real industrial I/O selection problems.

Section 5.3 is related to the NACRE (New Aircraft Concepts Research) model and considers four system configurations (mass cases variants). For each of them individually a optimal subset of sensors is chosen by the Method B which is given in 3.2.

In section 5.4, a further development on blended wing body (BWB) baseline is outlined. The ACFA 2020 model is a successor of NACRE design. The I/O selection Method D given in 3.4 is applied with respect to the parameter depending system. A grid of mass configurations is under scope and corresponding robust sensor subset is selected.

5.1 Evolution of flying vehicles. The BWB baseline as a future civil aircraft configuration

Allegedly the era of flying begun with first attempts to fly man-made objects in Greece (400 BC) and in China (200 BC). Constructions from Leonardo da Vinci ($15th$ century) were designed in several versions. With an aim to learn about the atmosphere, gases like hydrogen were discovered which led to an invention of hydrogen balloons. In $18th$ century the Montgolfier brothers launched their unmanned hot air balloon.

But it were the Wright brothers who built the first powered and controlled airplane. The first human flight took place on December 17^{th}, 1903, see Fig. 5.1 ([45]).

Figure 5.1: First heavier-than-air human flight by brothers Wright

Since then, during the aeronautical evolution, many baselines and configurations were designed and tested. Various airframe types were intuitively constructed. After time, the configuration with defined functions - fuselage to carry the passengers and cargo, wings to produce the lift and tail to ensure the stability earned more and more attention and it has been continuously developed and optimized into the today's conventional civil aircraft. Many attempts during airframe evolution were done in order to improve the aircraft attributes, as given in [34], see Fig. 5.2.

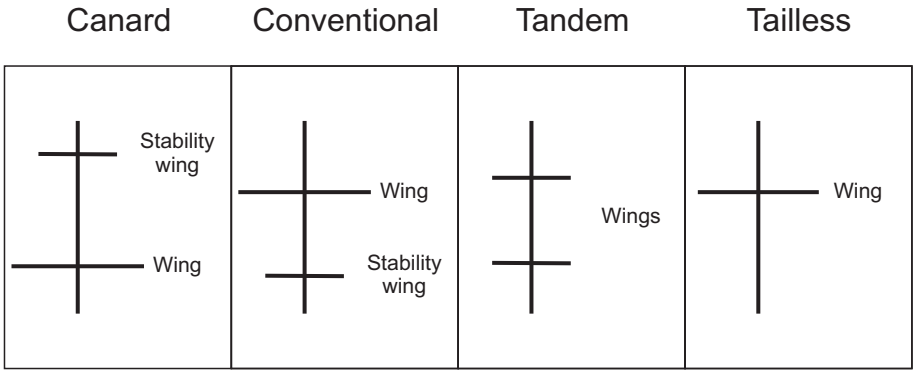

Figure 5.2: Basic airframe classification

Nowadays, modern Aircraft still remain at conventional airframe - the haul to carry passengers and cargo, wings to produce lift and vertical stabiliser to ensure vertical stability (see Fig. 5.3). Modern civil transport aircrafts have been precisely

Figure 5.3: Modern civil aircraft configuration

optimized in last decades focusing on efficiency, noise reduction and green propulsion technologies. Since the infrastructure of most airports in the world (mainly their taxis) are build for flying vehicles, which are not longer and brighter than 80 meters, the capacity of single haul concept is considerably limited. As shown on the Fig. 5.3, the second deck significantly increases the transport capacity. Taking one step further to increase the payload capacity even more, a horizontal extension of a fuselage would cover more of available space and markedly rise the transport capacity, improve costs and environmental flight aspects related to 1 passenger per nautical mile.

There were several attempts to integrate all functions into just one surface. Heading the flying wing concept, further designs were proposed. Smoothing the connection between wings and extended fuselage, ideally to leave out the vertical tail constitute a advanced aircraft frame. Such a concept is called *Blended Wing Body (BWB)*, see Fig. 5.4.

In this configuration, the thick aircraft body is connected to the wing in very smooth manner, whereby the profile is streamlined. Thus, the aircraft body contributes to generation of total lift and reduction of fuselage drag. The conventional fuselages designed to carry the passengers and cargo aerodynamically produce only little lift and significantly contribute to overall drag.

The BWB concept can be considered as a modification of tailless aircraft. How-

Figure 5.4: Blended Wing Body concept

ever, it can be constructed also with a tail, its definition depends only whether the fuselage and wings are blended or not.

If there would be completely no geometrical division between wing and fuselage, but the whole aircraft would have a form of a wing, such flying vehicle would be classified as a flying wing. In [46], this concept is called lift fuselage.

Already in later 80's a renaissance thoughts about new baseline concepts came into center of discussions within elite aeronautical engineers. As stated in [14], the first investigation and preliminary design of a subsonic passenger concept was conducted at McDonell Douglas with an aim to create and evaluate alternative configurations supposed to be set in service for long distance flights - 7000 nautical mile range at Mach of 0.85. Therein, a lateral extension of the aircraft body was carried out and three pressurized passenger compartments were designed.

Soon, the three tube concept was abandoned and the challenge turned into a new design of cabin vessel. Already at this very early stage of BWB concept development it was concluded, that compared with a conventional configuration aircraft sized for the same mission, the BWB concept is markedly lighter, indicates improved lift to

drag ratio and better fuel economy. This founding was a great motivation for further BWB baseline investigations.

Despite of constructional, flight stability, controllability, manoeuvrability, loss of thrust compensation effects, handling qualities and many other issues, the BWB baseline is very appealing to leading aeronautics institutions. Therefore, a significant attention is paid to this configuration.

5.2 NACRE configuration - brief overview

The term NACRE stands for *New Aircraft Concept Research* but within this work it is related to the specific aircraft model developed in the European project (see [9]). As shown in Fig. 5.5, the aircraft consists of wide fuselage, wings which are connected to the aircraft body not in absolutely smooth manner, and two vertical stabilization surfaces at the rear.

Figure 5.5: NACRE aircraft configuration

The horizontal stabilizer is here substituted by a large control surface between the vertical stabilizers. Based on internal project data ([48], [1] and [9]), additional modifications and extensions of the original model were performed. Masses for stiffness improvement were integrated as well as elements like cockpit, elevators and rudders, wing leading and trailing edges, landing gear, engines and pylons were replaced by concentrated masses. Non-structural masses as e.g. board equipment were

also integrated. Finally, the model was evaluated in various fuel load and pay load configurations. These models were prepared to include first 100 structural eigenmodes.

5.3 Selected I/O positions for NACRE model by Method B

In this text, the optimal I/O selection results for highly complex dynamical system - the NACRE model are presented. According to Sec.3.2, selected positions might be a good choice for control design. An effective performing control loop can help to reduce vibration of load-critical modes under standard operating conditions (modelled as turbulence excitation), thus decreasing dynamic loads and enabling further structural mass reduction. Robust control design methods, such as μ-synthesis approaches might be employed in the next steps of control design. However, to optimally design the control system, optimal selection and positioning of appropriate control inputs and measurement outputs is crucial. All critical modes have to be controllable and observable by the selected inputs and outputs. This application requires using all features outlined before: modal weighting to incorporate the turbulence excitation spectra and per-input weighting to account for varying flap efficiency across the wing span are both incorporated into the system model. Moreover, the system dynamics considerably changes over the aircraft parameters Θ which include aerodynamic parameters (Mach number, air speed) as well as other, structural parameters (fuel load, payload, and payload center-of-gravity position). In this study, the results are independently evaluated for four fuel cases since this parameter has the strongest influence on structure mode frequencies and shapes. The structure-only model, obtained by FE modelling and truncated to 60 elastic modes, has been transformed into modal form, using vertical forces and pitch moments along the wing trailing edges as inputs and vertical displacements as outputs. Then, a trailing edge flap model was set up, using an actuation efficiency estimation from a preliminary aerodynamic trim analysis and a consistent node load formulation. This model was used to generate a candidate set of actuators that resembled aerodynamic actuation, ensuring comparability within the input set. Fig.5.6 shows actuator selection results for four fixed fuel load configurations (00, 50, 22, and 44 indicate increasing fuel and payload mass from empty to full), using Method A [10] (normalized to a maximal value of 1) as well as by proposed Method B (see Sec.3.2)

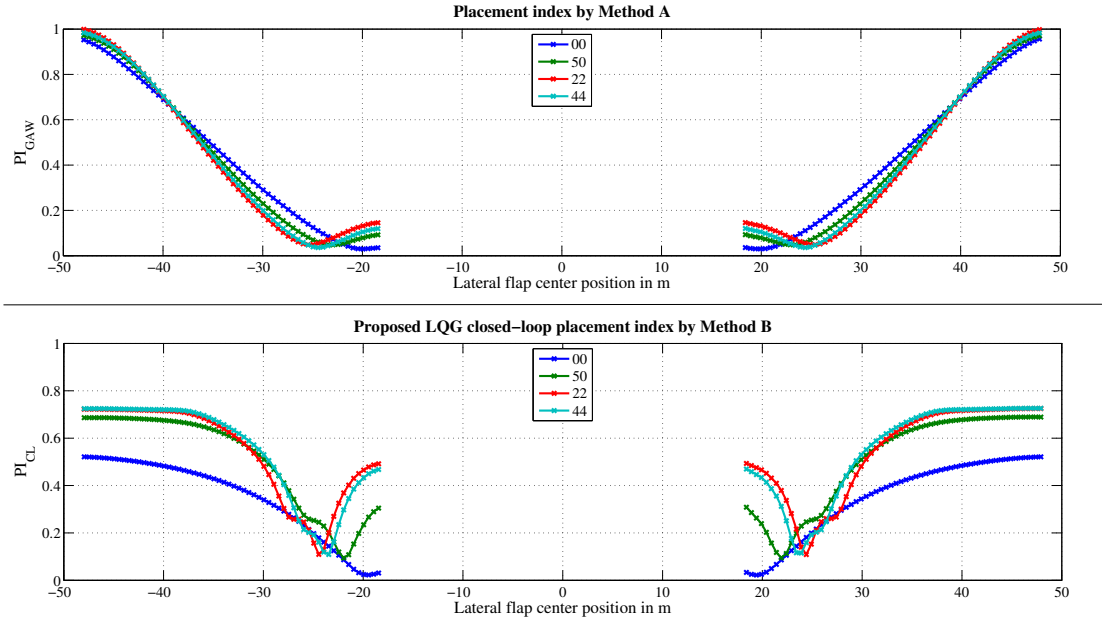

Figure 5.6: Actuator selection results by the Method A and Method B (single 2.5m flap, load criterion)

The results were obtained for the discretized fuel load/payload cases and fixed aerodynamic parameters for cruise flight (Mach Ma = 0.85, dynamical pressure p_0 = 15kPa used for span-wise flap efficiency estimation). The modal weighting has been done using mode gains of the disturbance transfer function (turbulence as a preliminary wind input, a wing-root load criterion proportional to vertical wing sensor displacements as output weighting). As actuator candidate set, a fine grid of modeled $2.5m$ trailing edge flaps has been considered. The flap center positions are plotted in the plots abscissa. These results show that, despite decreasing flap efficiency at the outer wing positions, these outmost flap positions are most favourable for load reduction with respect to turbulence excitation. However, comparing the two outcomes it is evident that the energy-based Method A ([10]) predicts higher actuator efficiency near the wingtips, while the closed-loop Method B indicates a saturation at the outmost $10m$ of the wingspan. Note that the criteria cannot be compared quantitatively, but the qualitative differences in the results extend the understanding of the problem, as the closed-loop faces fundamental limitations in time-domain performance while Method A due to its inherent open-loop nature, a controllability-based criterion cannot depict this class of limitations.

This might be crucial for aircraft engineering, because control surfaces placed closer to the aircraft body will have approximately the same effectiveness with re-

spect to disturbance attenuation, but the structural loads produced during aircraft manoeuvering might be significantly lower.

5.4 ACFA 2020 project - brief overview and project goals

The ACFA model is an advanced model of BWB aircraft. Several layout deferences in comparison to the NACRE model can be observed. As depicted on Fig.5.7, the fuselage transition into wing is considerably smoother. No rear vertical stabilizers are present. Propulsion units are designed at the rear top. Large winglets with vertical rudders and proof mass actuators are mounted on the wingtips. Along wings trailing edge a several control surfaces are designed. Two large high-lift control surfaces are at the rear of the fuselage.

The ACFA 2020 Project (see [35]) focuses on design of large BWB passenger aircraft, which will operate on mid- and long range missions. The required capacity of 400 passengers and beyond has been also formulated. Modified airframe shape and increased aerodynamic efficiency potentially lead to significant better fuel consumption properties related to passenger mile. Drag reduction, reduced structural weight, lower wetted area ratio ([36], [14]) as well as reduction by external noise by an advanced high-lift system ([23]) or shielding of the turbines pose a engineering challenge and evoke great expectations.
As outlined in the [35], the most relevant project objectives related to the ACFA 2020 Project can be summarized as follows

- 50 % reduction of fuel consumption and related CO_2 emissions per passenger mile
- Reduction of external noise by 4-5 dB and by 10 dB per operation in the short and long term, respectively
- Capacity of at least 400 passengers on a 7200 nautical mile missions in two class layauts
- Flight altitude 33000 feet and higher with a Cruise Mach number of 0.85
- For slow approaches a speed of less then 150 knots is required
- wingspan maximal 80 m
- the leading-edge sweep angle shall be 55° for the BWB center body

- the BWB center body's maximum relative thickness should not be more then 17%
- the span wise load distribution target is elliptic
- the payload weight (without fuel) up to 48720 kg

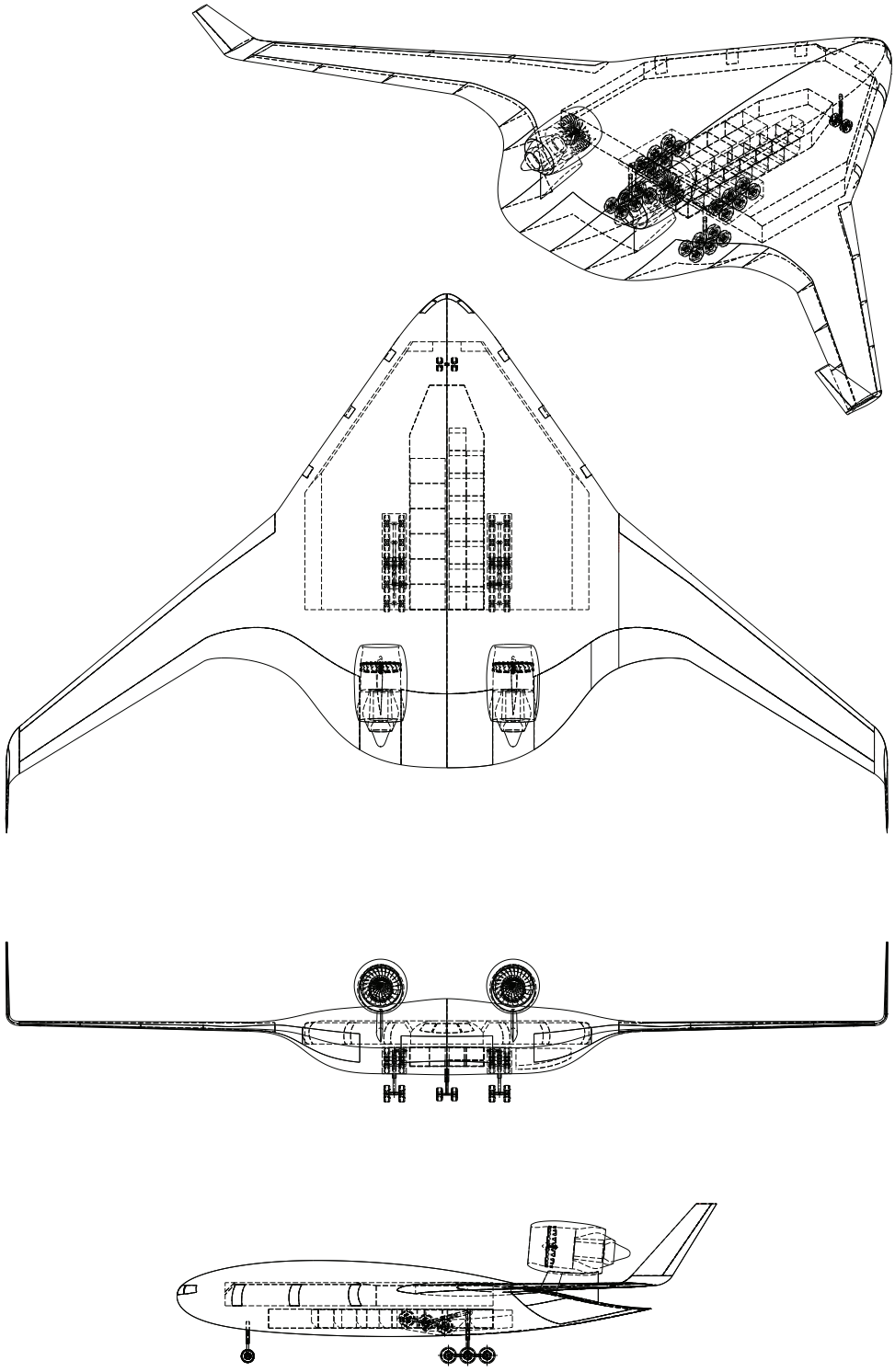

Figure 5.7: ACFA aircraft configuration

5.5 ACFA configuration and optimal I/O selection by the Method D

In this text, the ACFA model is briefly presented as well as an optimal I/O selection is outlined which allows to design a robustly performing controller. The Method D given in 3.4 is here applied. The ACFA model is a high complex system where the dynamics varies in dependence on a number of parameters like altitude, Mach number, payload, etc. The most relevant varied parameter related to structural dynamics is the fuel level, which ranks from full to almost empty. Three nominal fuel configurations are investigated: 100%, 50% and 0% of filling level. The fuel levels represent a grid of discretized nominal cases. Each fuel configuration consists of 852 states, 13 input channels and 576 outputs.

Input channels are the 8 control surfaces, 3 proof mass actuators, gust velocity and it's time derivative (see Tab. 5.1, Fig. 5.8). Outgoing from physical nature of last two channels, in this consideration, the input 13 is multiplied by s/(0.01s+1) (quasi dierentiator transfer function). In further consideration, the 12^{th} and 13^{th} input are unified (corresponding columns in the input matrix (B) and feed-trough matrix (D) are added). In this manner, the input set is reduced to 12 channels.

1	Flap 1
2	Flap 2
3	Flap 3
4	Flap 4
5	Flap 5 - outer aileron
6	Flap 5 in crocodile operating mode
7	Flap 5" - miniflap mounted into outer aileron
8	Winglet rudder
9	Front proof mass actuator (later only frontPMA)
10	Middle proof mass actuator (later only middle PMA)
11	Rear proof mass actuator (later only rear PMA)
12	Gust velocity input
13	Time derivative of gust velocity input

Table 5.1: ACFA system inputs

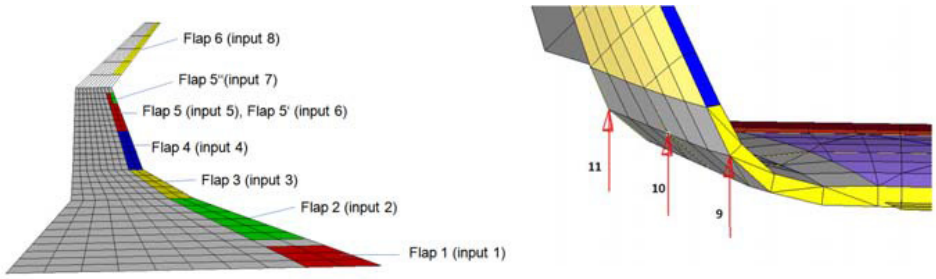

Figure 5.8: ACFA model inputs (figure designed by partners within ACFA2020 consortium, [6])

The output set is large. It consists of 576 outputs. They are classified according their usability.

1. Wing sensor set (sensors on the wing measure the vertical accelerations, sensors on the winglet measure the horizontal accelerations
2. Wing torque sensor set
3. Body roof sensor set (acceleration in vertical direction)

Table 5.2: ACFA sensor subsets

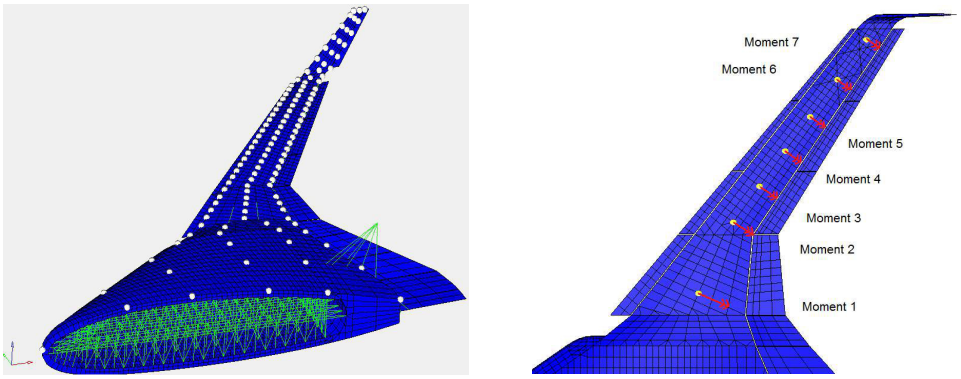

Figure 5.9: Left - Vertical acceleration sensors on body roof, wing and horizontal accelerometers on winglet. Right - modeled wing torque sensors in the wing structure. (Figure designed by partners within ACFA2020 consortium, [6])

The open loop transfer functions from the Gust input (weighted by von Karman Turbulence Model) to the Wing torque sensor set (see Fig.5.9 right) can be considered

as a quantity which represents the loads in the structure. Sensors measuring material stress (e.g. torque) inside the wing structure are not present in a real aircraft. Therefore, an optimal subset of vertical acceleration sensors on the wing structure has to be selected, which allow to design a robustly performing control loop for all fuel cases minimizing the material stress in the wing structure.

According to the Method D and it's execution depicted in Fig.3.6, basic eigenfrequencies of wing torque excited by gust have to be determined. They are listed in the Tab.5.3.

1. Structural mode	7,5 - 11 rad/s
2. Structural mode	18,5 - 24,5 rad/s
3. Structural mode	24,5 - 29,5 rad/s
4. Structural mode	31,5 - 33 rad/s

Table 5.3: ACFA eigenmodes of wing torque

The investigation based on phase difference properties is carried out in the next step. This results in narrower set of sensor candidates. Magnitudes of non eliminated candidates are evaluated. From the remaining set of candidates the most promising ones based on their open loop gain properties are selected. They are shown are shown in Fig.5.11 and Fig.5.11.

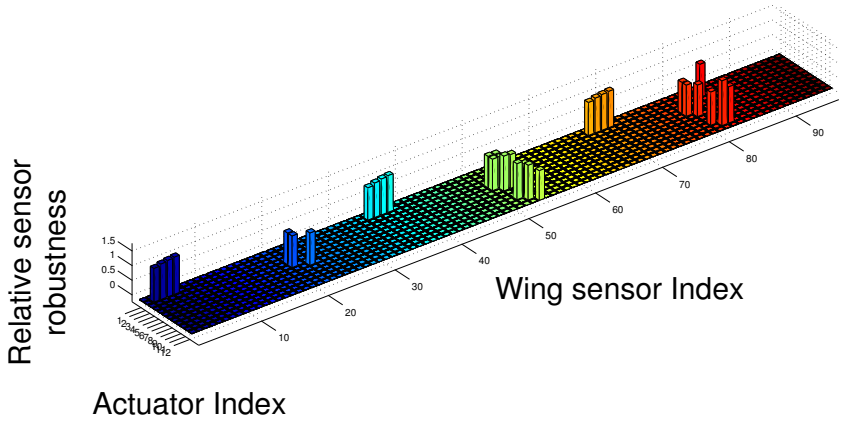

Figure 5.10: Selected sensor candidates by the Method D for robust control of 2^{nd} eigenmode

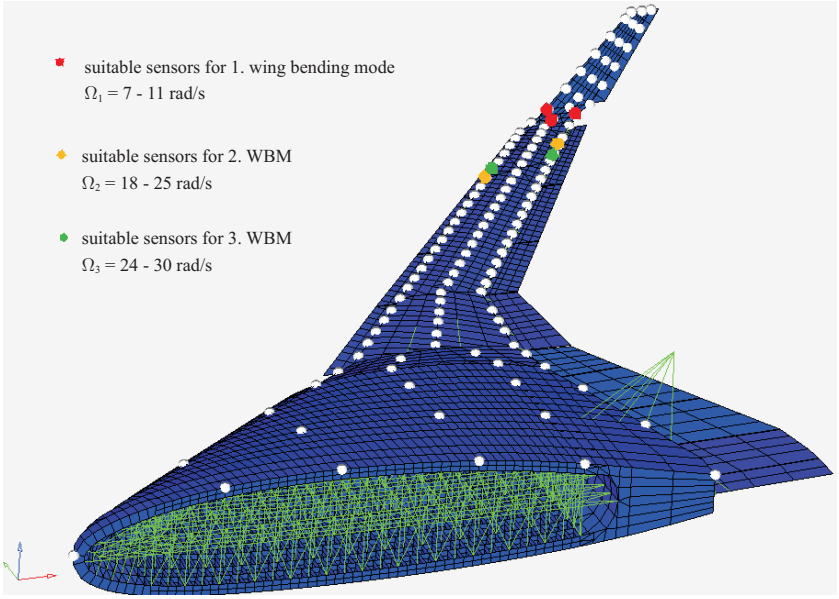

Figure 5.11: Selected sensors for robust control of 2^{nd} structural mode

Chapter 6

Summary

Since modern and environmental friendly engineering solutions count with continuous optimization, new approaches and methodologies are being developed. In this dissertation thesis, an optimal I/O selection problem is discussed which is an essential issue in regard to control design for flexible structures.

Each flexible system is characterized by it's structural properties and shows strong amplification of movement at certain excitation frequencies. These frequencies are called resonances or eigenfrequencies. There are a number of frequencies the flexible structure resonates at and it shape specific pattern of deformation. This pattern is called eigenmode.

Beside of some specific application like acoustics, etc., resonances pose a undesired behaviour. The modern engineering tries to solve this problem by control concepts which act against disturbances and damp the structure oscillations.

In this context, an active control loop consists of a flexible structure itself, sensor(s), actuator(s) and of a controller. The controller measures the dynamics of the flexible structure via sensors, computes control actions and executes them via actuators.

The basic prerequisite for a well operating control loop is to find optimal locations on the flexible structure for placing sensors and actuators. The sensor have to measure all relevant flexible structure dynamics while actuators have to transmit sufficient amount of energy into the structure to keep it in desired state. Redundancy is not an option because of high coasts and high complexity of control loop. Obviously, an optimal I/O selection task is an essential issue to be investigated before the main control design starts. This dissertation thesis focuses on the I/O selection problem and contributes with new methods.

Sec. 1 briefly summarizes this thesis, gives an introduction into the optimal I/O selection problem as well as an overview on structure of this work. A definition of flexible structures, structure modelling as well as a broad overview on state of the art I/O selection criteria are contained in Sec. 2.

In Sec. 3, particular I/O selection criteria are explained in more detail. Starting with the method A, an energy based criterion according to [10] is outlined. It compares the performance of each single actuator with performance of all available actuators. This results in a performance index which refers to actuator suitability for a control design. This criterion is used as a reference method for a validation of results evaluated by suggested selection techniques.

The Method B, which is presented subsequently, stands for a newly developed I/O selection method (see [20]). The performance index of particular I/O candidates is evaluated based on comparison of closed loop performances. Comparable LQG control designs with fixed $\mathcal{H}_2$ norm representing an energy potential available for the controller are carried out for each I/O candidate. In the following, the Method B is given in contrast with another I/O selection according to [4] which is considered as the Method C within this thesis. It utilizes a global optimization approach. Constrains related to closed loop stability and performance requirements are formulated via Linear Matrix Inequalities (LMI) and minimization problem is solved. Discussion on Method B and C can be also found in [19]. An integrated I/O selection technique called the Method D, which investigates systems with varying parameters, is discussed in the following. If the system parameters are slowly changing compared to the relevant system dynamics a fine grid of nominal models can be defined by approximating a continuously parameter dependent system by set of systems which have fixed parameter values valid only in the close neighbourhood of relevant operating points. This criterion allows to consider the system dynamics along all relevant operating range. It consists of three elimination substeps, where at each step those I/O candidates are eliminated which do not fulfil requirement stated therein. Elimination based on phase differences, magnitude properties and open loop gain capabilities are carried out. I/O candidates are selected which allow a performing robust control design. This I/O selection technique was introduced on 10^{th} International Conference on Motion and Vibration Control in Tokyo ([21]), moreover, it has been submitted to the Journal of System Design and Dynamics and published by Japan Society of Mechanical Engineers ([22]).

In Sec.4, Methods A, B and C are applied to a simple flexible structure in hinged-hinged configuration. The results are given and discussed. Method D deals with two different flexible beam configurations, namely, hinged-hinged and hinged-clamped set-ups, whereas robust I/O selection capabilities for system with different parameters is demonstrated. Given results indicate the best suited I/O candidates for robust control of both beam's configurations.

In Sec. 5, suggested Methods B and D are applied to a large industrial systems - to a blended wing body aircraft type. An short overview on the flight vehicle evolution is given. The call for investigation of new airframe types is formulated. The blended wing body with high transport capacity and thus high efficiency related to a passenger per nautical mile might be promising future alternative. This concept differs from conventional airframe considerably. Within this engineering challenge the robust control design for load alleviation and vibration reduction is one of main issues. The optimal I/O selection is performed for two aircraft models. The NACRE model is considered at different filling levels whereas for each of them an optimal I/O selection is individually computed by Method B. For another blended wing body model, called ACFA model within this thesis, a robust I/O subset for three nominal mass configuration, which demonstrate the parameter varying system, is sought by Method D. Selected candidates which allow to design a performing robust control loop are outlined.

Sec.6 summarizes content of this thesis. In Sec.7, extended information on ACFA 2020 Consortium is given. Goals and organizational structure are briefly discussed.

Chapter 7

Appendix - ACFA 2020 Project

7.1 Project overview

This dissertation thesis is based on research performed within the ACFA 2020 project. Therefore, it is meaningful to briefly introduce this project, it's motivation and main goals. The abbreviation ACFA 2020 stands for Active Control for Flexible 2020 Aircraft. This European project was grounded aiming to offer a new aircraft alternatives and consequently to investigate new flight vehicle concepts and their properties which might be set in service in the future. Due to the ecological tendencies in air traffic and continuously increasing number of passenger by air (see e.g. recent IATA forecast), the need for a green and efficient aircraft concepts becomes a very important issue at these days.

The European aeronautic community (ACARE - Advisory Council for Aeronautics Research in Europe) began to pioneer and analyze alternative aircraft baselines for civil transport purposes. Thus, the visions are clear, the new age of aviation and sustainable growth requires more affordable, cleaner, safer and more secure air travel.

The ACFA 2020 project assumes major changes in aircraft framing in order to reach defined goals. This project suggests the Blended Wing Body type aircraft (tailless aircraft concepts with ultra wide fuselage and blended wings) as a promising long term solution. Visualisation of this type of aircraft is depicted on Fig 7.1.

Fuel efficiency and subsequently reduction of CO_2 emmisions per passenger nautical mile, noise reduction, load reduction and thus reduction of structural weight are the main objectives. Using light weight structures requires an active structural control system. High level of handling qualities and ride comfort are mandatory.

Exterior noise, which needs to be reduced by 10 dB is planed to be scaled down by unconventional high lift design and by placing of the propulsion above the rear fuselage part.

Major constructional design issues have been already performed within the projects VELA and NACRE. During the construction design the need for more advanced and more sophisticated active control system has been identified but not addressed and solved. However, the Blended Wing Body type aircraft calls for new control architectures, it pose a great engineering challenges in regards to complexity of flight dynamics control algorithms, control design and optimization. In contrast to various cascade single channel control loops, in this case a highly coupled multichannel integrated control algorithm is under scope.

Project ACFA2020 information is summarized in its homepage [25] as well as in [35].

Figure 7.1: Blended Wing Body aircraft configuration

7.2 Structure

Following institutions have been involved in the research and technology development:

- EADS-Innovation Works
- Airbus
- Alenia Aerospace
- Hellenic Aerospace Industry S.A.
- Israel Aerospace Industry Ltd.
- DLR
- ONERA
- FOI
- Technical University Munich
- Vienna University of Technology
- Czech Technical University
- National Technical University Athens
- Bialystok Technical University

The project efforts have been distributed into four work packages.

- *Work package 1* had performed the definition of 450 passenger aircraft configuration. A Blended Wing Body and carry-through wingbox baselines were under scope at the beginning of the project. In a down-selection process based on a set engineering criteria, the Blended Wing Body baseline was selected for further investigations. A full composite structure has been assumed.
- *Work package 2* was developing a dynamic models for NACRE BWB aircraft and the new 450 passenger ACFA aircraft model. These aircraft models were completely prepared for the design and optimization of control laws. Work package 2 was responsible for delivering of models for atmospheric turbulence as well as for definition of comfort criteria with respect to vibrations.
- *Work package 3* has investigated the design of control architecture for the BWB baseline aircraft with focus on reduction of structural vibrations, elimination of unwanted rigid body motions and minimization of gust and manoeuvre loads.

After selection of optimal inputs and outputs, various robust as well as feed-forward and feedback techniques have been applied. Best performing control designs were highlighted and documented. The reduction of static and dynamic loads has been used as an input data for a resizing of the 450 passenger aircraft's structure at Work package 4

- *Work package 4* has investigated the impact of control concepts developed in Work package 3. The flutter analysis of the controlled aircraft as well as verification of the control concepts by use of high-fidelity aero-elastic tools has been performed. The resizing process of the 450 passenger ACFA aircraft based on the weight reduction allowed by active structural control might lead to it's fuel efficiency increase.

Bibliography

[1] Gust load alleviation on a large blended wing body airliner. *ICAS 2010, 27th international congress of the aeronautical sciences*, 2010.

[2] Al-Sulaiman and S. Zaman. Actuator placement in lumped parameter systems subjected to disturbance. *Computers and Structures*, 52(1):41–47, 1994.

[3] B.D.O. Anderson and J.B. Moore. *Optimal Control: Linear Quadratic Methods*. Prentice-Hall, 1989.

[4] S.A. Brodsky, A.V. Nebylov, and A.I. Panferov. Smart choice and location of sensors and actuators for aeroelastic object motion control. *Proc. 18th IFAC World Congress, Italy*, 2011.

[5] Y. Cao, D. Biss, and J.D. Perkins. Assessment of input-output controllability in the presence of control constraints. *Computers and Chemical Engineering*, 20(4):337–346, 1996.

[6] ACFA 2020 consortium. Active control of flexible 2020 aircraft - acfa 2020. *EU FP7 project no. 213321. URL: http://www.acfa2020.eu*.

[7] P. Daoutidis and C. Kravaris. Structural evaluation of control configurations for multivariable nonlinear processes. *Chemical Engineering Science*, 47(5):1091–1107, 1992.

[8] J.S. Freudenberg and D.P. Looze. Right half plane poles and zeros and design tradeoffs in feedback system. *IEEE Transactions on Automatic Control*, 30(6):555–565, 1985.

[9] J. Frota. Novel aircraft concepts. *2nd NACRE Conference, Greewich*, 2008.

[10] W. Gawronski. *Advanced structural dynamics and active control of structures*. Springer, New York, 2004.

[11] W. Gawronski and K.B. Lim. Balanced actuator and sensor placement for flexible structures. *International Journal of Control*, 65(1):131–145, 1996.

[12] D. Georges. The use of observability and controllability gramians of functions for optimal sensor and actuator location in finite-dimensional systems. In *Proceedings of IEEE Conference on Decision and Control*, volume 4, pages 3319–3324, 1995.

[13] R. Govind and G.J. Powers. Control system synthesis strategies. *A.I.Ch..E. Journal*, 28(1):60–73, 1982.

[14] Liebeck R. H. Design of the blended wing body subsonic transport. *Journal of Aircraft*, 41(1):10–25, 2004.

[15] A. Hać and L. Liu. Sensor and actuator location in motion control of flexible structures. *Journal of Sound and Vibration*, 167(2):239–261, 1993.

[16] T. Haniš and M. Hromčík. Optimal sensors placement and spillover suppression. *Mechanical Systems and Signal Processing 28, 367–378*, 2012.

[17] T. Haniš and M. Hromčík. Optimal sensor placement and elimination of undesirable mode shapes. *Proceedings of the European Control Conference 2009 * Budapest, Hungary*, August 23–26, 2009.

[18] T. Haniš and M. Hromčík. Information-based sensor placement optimization for BWB aircraft. *Preprints of the 18th IFAC World Congress Milano (Italy)*, August 28 - September 2, 2011.

[19] M. Hemedi, A. Schirrer, and M. Kozek. Comparison of LQ-optimal actuator / sensor selection approaches for flexible structure systems. *9th International Conference On Mathematical Problems In Engineering, Aerospace And Sciences: ICNPAA 2012", AIP Conference Proceedings; American Institute of Physics, College Park, MD, USA, 2012, ISBN: 978-0-7354-1105-0, S. 459 - 466*, 2012.

[20] M. Hemedi, A. Schirrer, C. Westermayer, and M. Kozek. Performance evaluation of an input/output selection criterion via normalized LQG closed-loop comparison. *17th IEEE Mediterranean Conference on Control & Automation, Thessaloniki, Greece*, 2009.

[21] M. Hemedi, A. Schirrer, C. Westermayer, and M. Kozek. Integrated input-output selection strategy for robust control of complex parameter varying systems. *10th International Conference on Motion and Vibration Control (MOVIC 2010), Tokyo, Japan*, 2010.

[22] M. Hemedi, A. Schirrer, C. Westermayer, and M. Kozek. Integrated input-output selection strategy for robust control of complex parameter depending

systems. *Journal of System Design and Dynamics 5, Special Issue of Motion and Vibration Control 2010 I (2011), 5; S. 1106 - 1118*, 2011.

[23] J. Hileman, Z. Spakovszky, M. Drela, and M. Sargeant. Airframe design for "silent aircraft". *In 45th AIAA Aerospace Sciences Meeting and Exhibit, Reno, Nevada, USA*, 2007.

[24] M. Hovd and S. Skogestad. Controllability analysis for unstable processes. In J. D. Perkins, editor, *Preprints IFAC Workshop Interactions between Process Design and Process Control*, pages 49–54. Pergamon Press, Oxford, 1992.

[25] http://www.acfa2020.eu/.

[26] I.A. Karnovsky and O.I. Lebed. *Free Vibrations of Beams and Frames - Eigenvalues and Eigenfunctions*. McGraw Hill Engineering Reference, McGraw-Hill, New York, 2004.

[27] E. Kreyszig. *Advanced Engineering Mathematics. 9th edition*. Wiley Int. Edition, John Wiley and Sons, Singapore, 2006.

[28] S. Kumar and J. H. Seinfeld. Optimal location of measurements in tubular reactors. *Chemical Engineering Science*, 33:1507–1516, 1978.

[29] H. Kwakernaak and R. Sivan. *Linear Optimal Control Systems*. Wiley-Interscience, 1972.

[30] J.R. Leigh. *Control Theory, 2nd Edition*. The Institute of Engineering and Technology, London, United Kingdom, 2008.

[31] S. Leleu, H. Abou-Kandil, and Y. Bonnasieux. Piezoelectric actuators and sensors location for active control of flexible structures. *IEEE Transactions on Instrumentation and Measurement*, 50(6):1577–1582, December 2001.

[32] W.S. Levine. *The Control Handbook*. CRC Press and IEEE Press, USA, 1996.

[33] K.B. Lim. Disturbance rejection approach to actuator and sensor placement. *Journal of Guidance, Control, and Dynamics*, 20(1):202–204, 1997.

[34] A. Lippisch. *The delta wing - history and development*. Iowa state University Press, 1981.

[35] A. Schirrer (Eds.) M. Kozek. *Modeling and Control for a Blended Wing Body Aircraft - A Case Study*. 2015.

[36] B. Mohr, D. Paulus, H. Baier, and M. Hornung. Design of a 450 passenger blended wing body aircraft for active control investigations. *Journal of Aerospace Engineering, 226(12):1513–1522, 2012*.

[37] B. Moore. Principal component analysis in linear systems: Controllability, observability, and model reduction. *IEEE Transactions on Automatic Control*, 26(1):17–32, 1981.

[38] M. Morari and G. Stephanopoulos. Studies in the synthesis of control structures for chemical processes - part 3: Optimal selection of secondary measurements within the framework of state estimation in the presence of persistent unknown disturbances. *A.I.Ch..E. Journal*, 26(2):247–260, 1980.

[39] H. Parkus. *Solid Body Mechanics (in German)*. 1995.

[40] S. Skogestad and I. Postlethwaite. *Multivariable feedback control*. John Wiley & Sons, 1996.

[41] S. Skogestad and I. Postlethwaite. *Multivariable Feedback Control*. John Wiley & Sons, 2. edition edition, 2005.

[42] Marc van de Wal and Bram de Jager. A review of methods for input/output selection. *Automatica*, 37:487–510, 2001. Survey Paper.

[43] C. Westermayer, A. Schirrer, M. Hemedi, and M. Kozek. An advanced criterion for optimal actuator and sensor placement on complex flexible structures. *IFAC Workshop on Control Applications of Optimization, Agora, Finland*, 2009.

[44] C. Westermayer, A. Schirrer, M. Hemedi, and M. Kozek. An advanced criterion for optimal actuator and sensor placement on complex flexible structures. In *IFAC Workshop on Control Applications of Optimization*, 2009.

[45] Wikipedia.org. Wright brothers.

[46] R. M. Wood and S. X. S. Bauer. Flying wings / flying fuselages. *39th AIAA Aerospaces Sciences Meeting & Exhibit*, AIAA - 2001-0311, 2001.

[47] K. Zhou, J.C. Doyle, and K. Glover. *Robust and optimal control*. Prentice-Hall, Upper Saddle River, NJ, 1996.

[48] P. Zuziak, Z. Šika, M. Valášek, T. Vampola, and T. Klimmek. Vibration control of flexible aircraft with respect to passengers comfort. *In Proc. ISMA 2010 - International Conference on Noise and Vibration Engineering*, 2010.